



**HAL**  
open science

## [Review] Metal nitrides as efficient electrode material for supercapacitors: a review

Ravikant Adalati, Meenakshi Sharma, Siddharth Sharma, Ashwani Kumar,  
Gaurav Malik, Rabah Boukherroub, Ramesh Chandra

### ► To cite this version:

Ravikant Adalati, Meenakshi Sharma, Siddharth Sharma, Ashwani Kumar, Gaurav Malik, et al..  
[Review] Metal nitrides as efficient electrode material for supercapacitors: a review. *Journal of Energy Storage*, 2022, 56 (part B), pp.105912. 10.1016/j.est.2022.105912 . hal-03842333

**HAL Id: hal-03842333**

**<https://hal.science/hal-03842333v1>**


Submitted on 14 Nov 2022

**HAL** is a multi-disciplinary open access archive for the deposit and dissemination of scientific research documents, whether they are published or not. The documents may come from teaching and research institutions in France or abroad, or from public or private research centers.

L'archive ouverte pluridisciplinaire **HAL**, est destinée au dépôt et à la diffusion de documents scientifiques de niveau recherche, publiés ou non, émanant des établissements d'enseignement et de recherche français ou étrangers, des laboratoires publics ou privés.

# Review article

## Metal nitrides as efficient electrode material for supercapacitors: A review


Ravikant Adalati <sup>a</sup>, Meenakshi Sharma <sup>a, b</sup>, Siddharth Sharma <sup>a, b</sup>, Ashwani Kumar <sup>a</sup>,  
Gaurav Malik <sup>a, c</sup>, Rabah Boukherroub <sup>d</sup>, Ramesh Chandra <sup>a</sup>, 

<sup>a</sup> Thin Film Laboratory, Institute Instrumentation Centre, Indian Institute of Technology Roorkee, Roorkee 247667, Uttarakhand, India

<sup>b</sup> Centre for Nanotechnology, Indian Institute of Technology Roorkee, Roorkee 247667, Uttarakhand, India

<sup>c</sup> Thin Film Laboratory, Department of Physics, Indian Institute of Technology Delhi, New Delhi 110015, India

<sup>d</sup> Univ. Lille, CNRS, Centrale Lille, Univ. Polytechnique Hauts-de-France, UMR 8520, IEMN, F-59000 Lille, France

 Corresponding author.

E-mail address: [ramesh.chandra@ic.iitr.ac.in](mailto:ramesh.chandra@ic.iitr.ac.in) (R. Chandra).

### ABSTRACT

Electrochemical supercapacitors as energy storage devices are trademarks in current electronic and industrial applications, as they are the source of top-notch power output. Supercapacitors supply fast power output, which is suitable to cover the energy demand of future electronic devices. Electrode materials of supercapacitors play an essential role in the electrochemical process of charge storage and determine the final device's cost and capacitive performance. Consequently, much attention has been paid to developing supercapacitor electrode materials to enhance energy storage performance and fulfill the high demand of current electronic devices. Electrode materials based on metal compounds such as metal oxides, metal nitrides, and metal carbides have been considered ideal for highly efficient electrochemical supercapacitors. Recently, many efforts have been devoted to metal nitride-based electrodes and their diverse compositions as they possess higher electrical conductivity, better corrosion resistance, electrochemical stability, and chemical reactivity. Electrode material, as well as the synthesis process of the electrode and assembling design of the final device, significantly impact the capacitive performance of the contrived electrochemical supercapacitor. This review gives a brief overview of supercapacitor configuration with methods for electrode synthesis and focuses mainly on the stable metal nitride components and their application as electrode materials for supercapacitors. Each element of the periodic table group has unique properties for electrochemical reactions, and stable metal nitrides can be synthesized with only a few elements of the periodic table. The electrochemical properties of metal nitride electrodes for supercapacitors depend upon the selected group of parent metals. In the conclusion of this review, we highlighted the recent trends and future aspects of metal nitride-based electrodes in energy storage devices.

### 1. Introduction

In the modern age, all the appliances for regular use require an energy system. In this advanced era, technology reached almost everywhere in the world, and this storm of technical development increases the demand for energy production and storage [1,2]. At present, fossil fuels are the major source of energy production, which is at the extinct level. Also, the use of fossil fuels produces various pollutants harmful to the environment. Researchers propose a new green energy solution to ensure the environment's safety and overcome the extinct fossil fuel problem. Green energy production uses natural resources, such as sunlight, wind, or water, without emission of any hazardous pollutants into the environment [3]. The green energy solution attracted enormous attention of researchers worldwide, who are working on

developing green energy and the effective ways to store that energy. There are several ways to store energy, out of which a good number of research groups are working on supercapacitors, as they are environmentally friendly and more effective than others with the possibilities of improvement. As the energy storage market has grown rapidly, supercapacitors are used in everyday appliances such as emergency doors of aircraft, memory backup systems, portable electronic devices such as cellular phones, uninterruptible power supplies (UPS), medical devices, and various micro-devices, especially electric vehicles (EVs) [4–6]. The EV is capable of being titled as a zero-emission transportation mode, which is expected to contribute significantly to solving the problems of global warming and environmental pollution [7–9]. A Ragone plot is presented in Fig. 1(a) to illustrate the energy density and power density

Note: Low-resolution images were used to create this PDF. The original images will be used in the final composition.

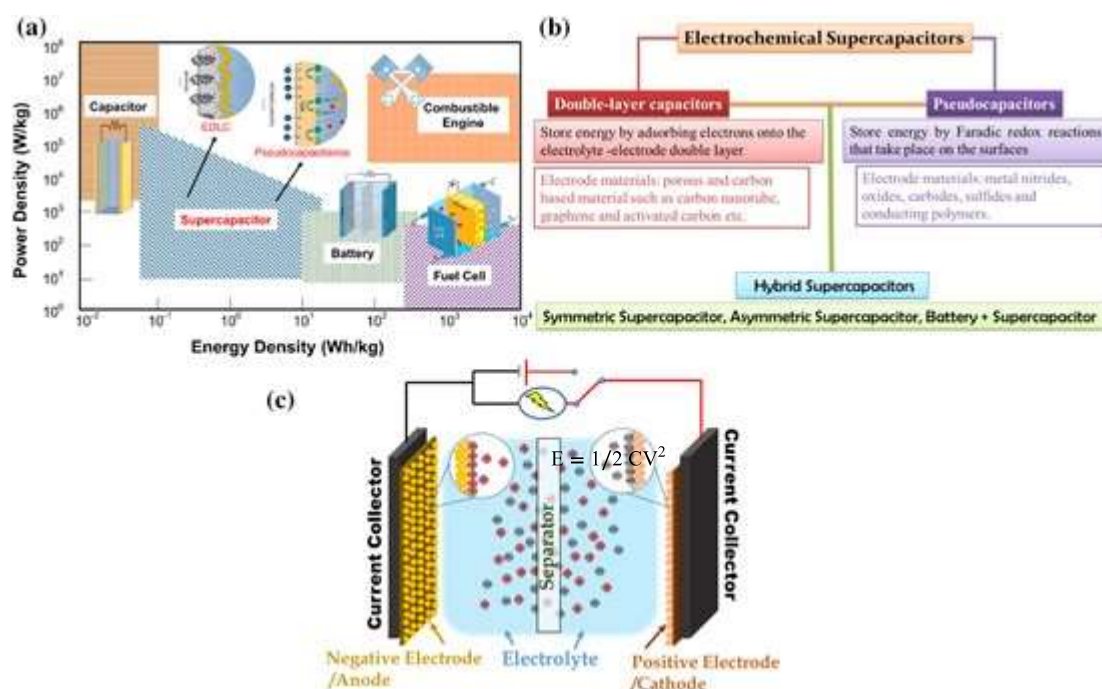


Fig. 1. (a) Ragone plot for efficiency comparison of various energy storage devices, (b) classification of electrochemical supercapacitors, and (c) schematic view of a supercapacitor structure.

comparison of batteries and fuel cells with supercapacitors (electrochemical capacitors).

Supercapacitors are categorized into two classes based on their charge storage mechanism: electric double-layer capacitors (EDLC) and pseudocapacitors. Fig. 1(b) summarizes the classification of supercapacitors on the basis of charge-storage mechanism and design/configuration. In EDLC, the charge is stored in the double layer capacitance, forming an electric double layer at the electrode electrolyte interface [10–14]. Commonly, carbon-based electrode materials are used as electrode materials in EDLC as they possess greater surface area, good electronic conductivity, and enhanced stability. These outcomes of carbon materials are the main characteristics of EDLC [15–19]. In pseudocapacitors, the charge is stored in the chain of redox reactions that are fast and reversible [20–22]. There are three types of reactions for charge storage in pseudocapacitors, (i) underpotential deposition, in which the charge is stored by ion deposition on metal/electrolyte interface negative to their redox potential, (ii) surface redox reactions, which store charge by chemical reaction across interface layer of electrode/electrolyte, and (iii) intercalation/deintercalation of ions in the electrode [23–25]. Metal compounds (metal sulfides, metal oxides, and metal nitrides) or conducting polymers are electrode materials commonly used for the pseudocapacitive storage mechanism. In the future, these metal compound materials/conducting polymers will be able to store electricity of tens to hundreds of times greater than carbon-based double-layer capacitors [26].

Commonly, supercapacitors suffer from low energy density compared to conventional batteries and fuel-cells. However, there are several designs/configurations for assembling supercapacitor devices (Fig. 1(b)) to overcome the problem of low energy density and limited operating voltage range. The appropriate designs/configurations to enhance the performance of supercapacitors are asymmetric, symmetric and hybrid supercapacitors. The latest type of supercapacitor uses electrodes based on different charge storage mechanisms, known as hybrid or asymmetric supercapacitors. These supercapacitors generated enormous attention from the research community due to their outstanding performances. An asymmetric supercapacitor (ASC) is one type of hybrid supercapacitors, which is a potential alternative to improve the energy density problem of the supercapacitor. Energy density ( $E$ )

is dependent on the square of applied voltage ( $V$ ) and capacitance ( $C$ ) of the supercapacitor, as per the Eq. (1) [27–30]:

$$E = 1/2 CV^2 \quad (1)$$

Thus,  $E$  is directly affected by the broadening of the working voltage window and capacitance. This broadening of operating voltage windows can be achieved by merging nanostructured-based active electrodes, having voltage windows adjacent to each other with opposite signs (negative and positive) in the identical electrolyte. So for the asymmetric supercapacitor, one acts as a positive electrode while the other as a negative electrode. Electrode materials like transition metal compounds with suitable electrolytes can help in enhancing the capacitance value. The supercapacitor device contrived in any configuration comprises three essential components: a positive electrode, a negative electrode, and an electrolyte, as shown in Fig. 1(c). All of these parts of the supercapacitor have their importance and effect on electrochemical performance. The impacts of electrolyte and electrode material on the electrochemical performance of the supercapacitor are discussed below:

Electrolytes for supercapacitors can be categorized into aqueous and non-aqueous. Due to the broader electrochemical range, organic electrolytes nowadays are the solid choice. Even though organic electrolytes can operate at voltages of up to 3 V, they suffer from being flammable and hazardous [31,32]. The practical energy density of an organic electrolyte-based supercapacitor is not high and is mostly lower than 5 Wh kg<sup>-1</sup>. Due to the large size of organic molecules, capacitance is not large enough.

Ionic liquids possess aqueous and organic electrolyte characteristics, such as high ionic conductivity and a wide operating potential range up to 35 V. Ionic liquids-based electrochemical energy storage systems offer good conductivity, nonflammability, and high thermal stability with a wide voltage window. The relatively high cost compared to conventional organic solvents and electrolyte salts, and complex synthesis process hamper the widespread use of ionic liquids in supercapacitors [33,34]. Aqueous electrolytes feature several advantages over organic electrolytes including low cost, easy assembling process, and inflammability. In addition, aqueous electrolytes exhibit high ionic conductivity (two orders of magnitude greater than that of

organic electrolytes), confirming high rate-capability and, therefore, greater capacitance and power density [35–38]. As the electrode directly makes contact with the electrolyte without a surface layer, at the electrolyte-electrode interface, the charge transfer occurs without interference from the surface layer. Water is considered as an excellent solvent for electrolytes, because water decomposition into hydrogen and oxygen products (water electrolysis) do not pollute the electrolyte. Water can also make supercapacitors resistant to overcharging by generating oxygen (OER) and hydrogen (HER) at the positive and negative electrodes, respectively. Hydrated ions are much smaller in size than their organic counterparts, but their capacitance is comparatively high. Therefore, with a low operating voltage window of the aqueous electrolyte, top-notched energy and power density can still be achieved.

Furthermore, constructing top-notch-performing electrode material is critical for improving energy density without sacrificing power density or cycle lifespan. Nanostructured-based electrode materials are an excellent choice for supercapacitors, as they possess remarkable properties for efficient capacitive performance. Currently, different types of metal compounds are reported for supercapacitor electrodes. These metal compound-based electrodes received massive attention, because of their unique physico-chemical properties. Metal compounds-based electrodes are promising and active electrode materials for improving the performance of supercapacitors. Several metal compounds such as metal carbides, metal sulfides, metal oxides, and metal nitrides have been investigated in the scientific literature [7,30,39–46]. These different types of electrodes have some benefits as well as drawbacks [47, 48]. For example, metal oxide-based electrodes feature a high capacitance value, but their relatively poor electrical conductivity obstructs their electrochemical-capacitive performance. The stability and electrical conductivity of metal oxides are poor, despite continuous progress in supercapacitor performance [49,50]. In contrast, metal nitrides bestow performance over the other compounds; for example, the electrical conductivity of TiN is  $4.5 \times 10^6 \text{ S m}^{-1}$ , while the that of  $\text{TiO}_2$  is  $10^{-8} \text{ S m}^{-1}$  [51]. The drastic difference in the value of the electrical conductivity has switched the attention of researchers towards metal nitrides as promising materials for supercapacitor application. Nonoxide materials, like metal carbide and metal sulfide-based electrodes, have high electrical conductivity and superior hydrophilic nature. For instance, 1 T  $\text{MoS}_2$  and  $\text{Ti}_3\text{C}_2$  recorded a high volumetric capacitance value of  $650 \text{ F cm}^{-3}$  and  $900 \text{ F cm}^{-3}$ , respectively. However, they are restricted to the highest sweep rate of  $1 \text{ V s}^{-1}$  [52,53]. Hence, there is an urge to look for alternative electrode materials for pseudocapacitors. Because of this, metal nitrides have become a promising substitute for oxides. The electrical conductivity and pseudocapacitance of metal oxides deficient in oxygen have improved supercapacitor performance. On the other hand, the incorporation of electron donor features in metal oxides or the conversion of an oxide to a nitride can enhance capacitance and increase hydrogen and oxygen evolution overpotentials. Therefore, nitrogen substitution by replacing oxides or hydroxides entirely affects the electrochemical properties. When transition metal nitrides are formed, the d-band of the parent metal is altered. The d-band alteration causes an increase in the density of states (DOS) near the Fermi level [54,55]. Transition metal nitrides with these DOS changes exhibit catalytic activities similar to noble metals, unlike their parent metals [56,57]. Metal nitrides display improved electronic, catalytic, and magnetic properties compared to parent metals, due to the presence of electron-rich metal-nitrogen bonds [58]. In general, when metal nitrides are involved in the electrochemical/catalysis process, two major effects can be bought into consideration [41,59,60].

- (i) Ligand effect: Metal nitrides have a dissimilar electronic structure compared to the parent metal. In metal nitrides, the non-metal acquires charge from the metal, and the metal d-states with non-metal sp-states tend to hybridization and metal-metal lattice spacing expansion. The electronic structure alteration enhances the chemical reactivity of the parent metal, allowing reactants and products to be

adsorbed with similar strength to noble metals, improving the selectivity of the reactions.

- (ii) Ensemble effect: The surface nitrogen can significantly lower the available number of sites on the metal surface. By varying the metal to nitrogen ratio, this effect can be changed. In metal-nitrogen bonding, the d-band structure of the parent metal changes/shrinks, that basically changes the activity of the catalytic site and allows transition metal nitrides to achieve noble metal-like electrocatalytic activity. Depending on their bonding, the nitrides can be classified as follows:
  - (i) The alkali and alkaline earth group metal nitrides form an ionic bond. Due to the ionic bonding of Li and  $\text{N}_2$ ,  $\text{Li}_3\text{N}$  exhibits exceptional ionic conductivity [61].
  - (ii) The icosagens and crystallogens group metal nitrides form a covalent bond. They are semi-conductive or nonconductive, and exhibit good hardness and higher melting point [62].
  - (iii) Transition metal nitrides display versatile physical and chemical properties due to the formation of ionic, covalent, and metallic bonding [63,64].

These distinct bonding and structures incite exceptional physicochemical properties of the final metal nitride compounds such as multiple crystal structures and valence states, superb electrical conductivity which is comparable to the metals and higher than their oxides while providing rich redox chemistry for improved electrochemical activities. All of these properties are essential for better performing electrode material [65–67].

Research done so far directly implies the bestow performance of metal nitrides over other compounds. A periodic table is depicted in Fig. 2(a) for the selection of metal from any group (I, II, III, IV and transition metals) to synthesize metal nitride electrodes. Fig. 2(b) presents the approved methods to synthesize metal nitride electrodes. Several methods have been conveyed for the developing of metal nitride-based electrodes, which can be classified into three categories [22]: (i) chemical route synthesis (hydrothermal, sol-gel, template method or temperature controlled reaction/reduction procedures) of metal oxide powder, followed by nitration or annealing in an ammonia atmosphere; electrode preparation was achieved by casting a layer of binder and metal nitride powder slurry over the substrate, (ii) electrochemical reaction in the presence of catalyst and precursor, to deposit metal oxide layer on the substrate followed by nitridation to acquire metal nitride electrodes, and (iii) physical/chemical vapour deposition in the  $\text{Ar}_2 + \text{N}_2$  or  $\text{N}_2$  atmosphere of metal nitride film on the substrate in absence of any binder or catalyst using pulsed laser deposition (PLD), magnetron sputtering, chemical vapour deposition (CVD), thermal vapour deposition (TVD) and spray coating [47,62,68–78]. Some of the recently reported electrodes are summarized in Table 1 to compare all the metal nitride-based electrodes for supercapacitor devices and their performance. This report briefly reviews stable metal nitride electrodes and discusses current challenges and future strategies for energy storage devices.

## 2. Transition metal nitrides (TMNs)

Transition metal nitrides (TMNs) are interstitial metallic compounds wherein the nitrogen atom is integrated into the parent metal's interstitial sites, endowing them with covalent and ionic properties. A unique electronic structure, an outstanding mechanical robustness, an enhanced chemical stability, and fascinating electrocatalytic activity distinguish these materials. TMNs have drawn remarkable research attention in several applications, mostly for energy storage and conversion [79–81]. As a general rule, TMNs own metallic, ionic, and covalent

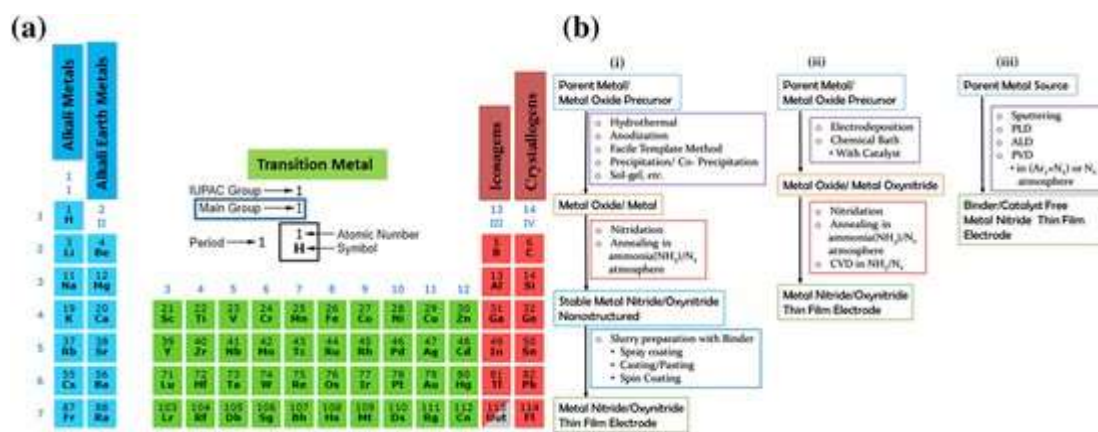


Fig. 2. (a) Periodic table for the selection of the metal to develop stable nitride-based electrodes, and (b) generally adopted synthesis methods for metal nitride electrodes.

bonding simultaneously, where the M–N bonding causes the parent metal's lattice to expand and its d-bands to constrict [63,82–84]. Because of the shortage of the d-band and the higher density of states (DOS) near the Fermi level of TMNs, they can exhibit noble metal-like behavior in electrocatalysis process and facilitate better adsorption of reactants/ions onto their surfaces, making them attractive candidates for electrochemical energy storage and conversion [85,86]. In addition, they can be used in a wide pH range due to their chemical inertness. Though TMNs exhibit top-notch electrochemical activity, they have limited electrochemically active sites in their bulk form, meaning that TMNs are not as efficient for catalysis as well as for energy storage. Nano-engineering of TMNs with morphologies that facilitate ion mass transfer, reduce electrolyte diffusion distance, and improve their capacitive performance is of great importance for enlarging their specific surface area and enriching them with active sites. So far, plentiful TMNs composed of transition metal group have been successfully explored as electrode materials for electrochemical supercapacitors, Shah et al., 2014 reported the large surface area of Mo<sub>x</sub>N-based materials with high porosity and capacitance up to 275 F g<sup>-1</sup> when the electrode is cycled in aqueous H<sub>2</sub>SO<sub>4</sub> or K<sub>2</sub>SO<sub>4</sub> electrolytes. This electrode also shows high stability over long cycles [87]. Achour et al. (2015) reported the microsupercapacitor electrode of TiN with controlled porosity, a superior volumetric capacitance of 146.4 F cm<sup>-3</sup>, and outstanding cycling stability over 20,000 cycles in the neutral electrolyte of potassium sulfate [88]. A research group (Eustache et al., 2013) reported the superior specific capacitance of 850 F g<sup>-1</sup> and stability of vanadium nitride (VN) electrode in 1 M KOH electrolyte [89]. Another research group (Choi et al., 2015) reported the pseudo-capacitive behavior of VN in 1 M KOH electrolyte with optimum energy (0.7 μW h cm<sup>-2</sup>) and maximum power densities (28 mW cm<sup>-2</sup>) [90]. However, according to Balogun et al. (2016), Ni<sub>3</sub>N nanosheet-based electrode grown on a 3D carbon cloth shows a high capacitance of 593 mA h g<sup>-1</sup> with excellent stability [91]. In addition, Wei et al. have prepared TiN and VN as the supercapacitor electrode materials, both of which showed boosting capacity and excellent stability [92]. Moreover, Sridhar and coworkers (2019) reported that manganese nitride decorated reduced graphene oxide (MnN@rGO) as an electrode in supercapacitors and EMI-protecting applications [93]. This electrode shows a high capacitance value of 639.2 F g<sup>-1</sup> at scan rates of 10 mVs<sup>-1</sup> in 1 M Na<sub>2</sub>SO<sub>4</sub> aqueous electrolyte with superior stability when employed as an electrode in supercapacitors. Recently, Cui and coworkers (2015) reported a 3D Nb<sub>4</sub>N<sub>5</sub> nano-channels/Nb foils electrode with a higher capacitance of 225.8 mF cm<sup>-2</sup> and excellent stability after 2000 cycles due to high porosity and conductivity [94]. Transition metal nitrides such as Ti N [95], Zr N [96], V N [97], Nb N [98], Ta N [99], Cr N [100], Mo N [101], W<sub>2</sub>-N<sub>3</sub> [102], Mn N [103], Fe N [104], Co N [105], Ni N [106], and Cu N [107] are the stable metal nitride electrodes for supercapacitors applications because of their low cost, excellent electronic conductivity,

high stability at higher temperatures, and good chemical resistance.

### 2.1. Vanadium nitride (VN)

For supercapacitors, the most well-studied transition metal nitride is vanadium nitride (VN) due not only to its greater capacitance, but also to its better electrical conductivity (about  $1.6 \times 10^6$  S m<sup>-1</sup>). In addition to its several oxidation states (II–V), great electrical conductivity, high melting point (2300K), enhanced thermal stability, and wide operating voltage in the negative region, VN is a good candidate as an electrode material. Due to a superb theoretical capacitance value of 1340 F g<sup>-1</sup>, VN-based supercapacitors have drawn considerable attention. However, the experimentally-determined capacitance of this material is far lower than its theoretical value. Therefore, a huge amount of work was devoted to increase the practical capacitance value of the VN electrode [108].

Lu et al. contrived an asymmetric quasi-solid-state supercapacitor using VO<sub>x</sub> and VN nanowires coated porous carbon cloth electrode that exhibited great energy density. Fig. 3(a) presents the digital images of VO<sub>x</sub> and VN nanowires coated porous carbon-cloth electrodes. Fig. 3(b) displays the surface SEM micrograph of VN, confirming the uniform growth of the electrode material via hydrothermal method. VN preserved nanowire-like structure even after nitridation process (postannealing of VO<sub>x</sub> in ammonia at 600 °C for 1 h). Fig. 3(c) depicts the CV curves and Fig. 3(d) presents the specific-capacitance value of VN nanowire electrode calculated at several scan rates in the presence of LiCl/PVA gel-type electrolyte. VN nanowire featured a combined contribution of EDLC and pseudocapacitance, as Faradaic reactions occurs at the surface of the VN electrode, which is corroborated by the asymmetric shape of the CV curves. SEM micrographs of VN nanowires embedded in LiCl/PVA post 10,000 charging cycles, shown in Fig. 3(e), confirms the better electrochemical performance and preservation of the nanostructure of VN. The use of LiCl/PVA gel-type electrolyte significantly improved the electrochemical stability of VN nanowires. This VN electrode attained an outstanding capacitance value of 298.5 F g<sup>-1</sup> at the scan rate of 10 mV s<sup>-1</sup> and offered 95.3 % capacitance retention after 10,000 charging cycles [109].

Chen et al. contrived novel mesoporous VN composite array coupled to poly (3, 4-ethylene dioxythiophene), also known as PEDOT, as a flexible electrode for solid-state SC. The hydrothermal-nitridation method was utilized for the preparation of mesoporous VN nanosheets with cross-linked nanoparticles of 10–50 nm in size. A PEDOT shell was electrodeposited over the VN to form efficient VN/PEDOT flexible-arrays with improved electrochemical stability. These designed VN/PEDOT flexible arrays provided a remarkable cycle shelf-life with 91.5 % capacitance-retention even after 5000 charging-cycles at 10 A g<sup>-1</sup>. By



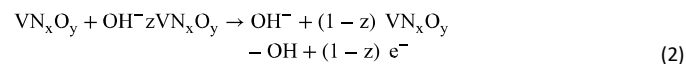
**Table 1**  
Metal nitride-based electrode materials for electrochemical energy storage application.

Entry	Electrode material	Synthesis method	Electrolyte	Capacitance	Voltage window	Reference
1.	VO <sub>x</sub> /VN	Hydrothermal growth	5 M LiCl	298.5 F g <sup>-1</sup> at 10 mV s <sup>-1</sup>	-1.2 to 0 V	[109]
2.	VN/PEDOT	Wet chemical	1 M KOH	226.2 F g <sup>-1</sup> at 1 A g <sup>-1</sup>	-1.2 to -0.2 V	[110]
3.	VN	DC magnetron sputtering	1 M KOH	422 F g <sup>-1</sup> at 10 mV s <sup>-1</sup>	-1.2 to 0 V	[111]
4.	VN/C	Multi-phase polymeric strategy	6 M KOH	392 F g <sup>-1</sup> at 0.5 A g <sup>-1</sup>	-1.2 to 0 V	[112]
5.	VNNDs/CNSs	Nitridation	1 M KOH	1203.60 F cm <sup>-3</sup> at 1.10 A cm <sup>-3</sup>	-1 to -0.2 V	[184]
6.	Cr-doped VN	Co-sputtering	1 M KOH	190 mF cm <sup>-2</sup> at 10 mV s <sup>-1</sup>	-1 to 0 V	[113]
7.	VN@SS and γ-Mo <sub>2</sub> N@SS	DC magnetron sputtering	1 M Na <sub>2</sub> SO <sub>4</sub>	85.50 F g <sup>-1</sup>	0 to +1.4 V	[114]
8.	Pt-Cr <sub>2</sub> N	DC magnetron sputtering	1 M Na <sub>2</sub> SO <sub>4</sub>	557 F g <sup>-1</sup> at 1 mA cm <sup>-2</sup>	0 to +1.2 V	[115]
9.	Cr <sub>2</sub> O <sub>3</sub> /CrN	Hydrothermal produced -Cr <sub>2</sub> O <sub>3</sub> annealed in ammonia atmosphere	1 M KOH	333.2 F g <sup>-1</sup> at 10 mV s <sup>-1</sup>	0.1 to -1 V	[116]
10.	Porous CrN	Oblique angle magnetron sputtering	0.5 M H <sub>2</sub> SO <sub>4</sub>	17.7 mF cm <sup>-2</sup> at 1.0 mA cm <sup>-2</sup>	0 to +0.8 V	[117]
11.	3D CrN@ nitrogen-doped carbon nanosheet arrays	Reactive sputtering	0.5 M H <sub>2</sub> SO <sub>4</sub>	132.1 mF cm <sup>-2</sup> at 1.0 mA cm <sup>-2</sup>	0 to +0.8 V	[118]
12.	Co <sub>3</sub> N	Reactive magnetron sputtering	6 M KOH	47.5 mC cm <sup>-2</sup> at 1.0 mA cm <sup>-2</sup>	-0.4 to 0.2 V	[120]
13.	Ni-doped Co-Co <sub>2</sub> N	Simple thermal annealing	1 M KOH	361.93C g <sup>-1</sup> at 2 mA cm <sup>-2</sup>	0 to 0.6 V	[121]
14.	CoN	Magnetron sputtering	1 M Na <sub>2</sub> SO <sub>4</sub>	520 F g <sup>-1</sup> at 0.5 mA cm <sup>-2</sup>	-1 to 0 V	[122]
15.	Graphene/LiNO <sub>3</sub> composites	Mixture of LiNO <sub>3</sub> and graphene burning and grinding	6 M KOH	3339.7 F g <sup>-1</sup> at 1 mV s <sup>-1</sup>	0 to 0.5 V	[153]
16.	Li <sub>3</sub> N	Slurry-cast	1.0 M LiPF <sub>6</sub>	70 mAh g <sup>-1</sup> at 50 mA g <sup>-1</sup>	2 to 4.2 V	[154]
17.	Li <sub>3</sub> N	N <sub>2</sub> plasma activation	1 M LiPF <sub>6</sub>	141 mAh g <sup>-1</sup> at 0.56 mAh cm <sup>-2</sup>	3 to 4.2 V	[148]
18.	W <sub>2</sub> N	Magnetron sputtering	1 M KOH	550 mF cm <sup>-2</sup> at 2 mV s <sup>-1</sup>	-0.9 to -0.3 V	[125]
19.	W <sub>2</sub> N	Magnetron sputtering	1 M H <sub>2</sub> SO <sub>4</sub>	163 F g <sup>-1</sup> at 0.5 mA cm <sup>-2</sup>	-0.3 to 0.8 V	[126]
20.	WN-rGOF	Hydrothermal + nitridation	PVA/H <sub>3</sub> PO <sub>4</sub> gel	16.29 F cm <sup>-3</sup> at 0.05 A g <sup>-1</sup>	0 to 0.8 V	[127]
21.	Mn <sub>3</sub> N <sub>2</sub>	DC magnetron sputtering	1 M (KOH, KCl, Na <sub>2</sub> SO <sub>4</sub> )	118 mF cm <sup>-2</sup> , 68 mF cm <sup>-2</sup> , 27 mF cm <sup>-2</sup> at 10 mV s <sup>-1</sup>	-0.4 to 0.4 V	[129]
22.	MnN@rGO	Microwave-Nitridation	1 M Na <sub>2</sub> SO <sub>4</sub>	639.2 F g <sup>-1</sup> at 10 mV s <sup>-1</sup>	0.0 to 1.0 V	[93]
23.	MnN	Nitridation	1 M Na <sub>2</sub> SO <sub>4</sub>	1044.3 F cm <sup>-3</sup> at 1 A g <sup>-1</sup>	-1.0 to 0.6 V	[130]
24.	TiN	DC reactive sputtering	1 M KCl	4.4 mF cm <sup>-2</sup> at 0.05 mA cm <sup>-1</sup>	-0.6 to 0.4 V	[132]
25.	TiN	Reactive sputtering	0.5 M K <sub>2</sub> SO <sub>4</sub>	4.25 mF cm <sup>-2</sup> at 100 mV s <sup>-1</sup>	-0.2 to 0.6 V	[88]
26.	TiVN (1:1 ratio)	Reactive co-sputtering	1 M KOH	15 mF cm <sup>-2</sup> at 2 mV s <sup>-1</sup>	-0.6 to 0.4 V	[133]
27.	CNT-TiN	ALD	0.5 M H <sub>2</sub> SO <sub>4</sub>	81 mF cm <sup>-2</sup> at 10 mV s <sup>-1</sup>	-0.1 to 0.5 V	[134]
28.	TiN/Ti	Electrodeposition	1 M LiClO <sub>4</sub>	53.66 mF cm <sup>-2</sup> at 6.66 mA cm <sup>-2</sup>	0 to 1.6 V	[135]
29.	γ/δ-Mo <sub>2</sub> N	Ammonolysis	0.5 M K <sub>2</sub> SO <sub>4</sub> (and 0.5 M H <sub>2</sub> SO <sub>4</sub> )	275 F g <sup>-1</sup> (and 202 F g <sup>-1</sup> ) at 2 mV s <sup>-1</sup>	-0.7 to 0.1 V (-0.7 to 0 V)	[87]
30.	MoN	Electrodeposition	1 M LiOH	467.6 mF cm <sup>-2</sup> at 5 mA cm <sup>-2</sup>	-1.1 to -0.1 V	[144]
31.	Ni <sub>2</sub> Mo <sub>3</sub> N	Hydrothermal process	6 M KOH	264C g <sup>-1</sup> at 0.5 A g <sup>-1</sup>	0 to 0.5 V	[145]
32.	MoN	Nitridation	0.5 M H <sub>2</sub> SO <sub>4</sub>	16 mF cm <sup>-2</sup> at 50 mV-s <sup>-1</sup>	-0.5 to 0 V	[131]
33.	BN/CNT/PANI	Chemical	1 M KCl	515 F g <sup>-1</sup> at 1 A g <sup>-1</sup>	0 to 0.8 V	[160]
34.	h-BN/RGO	Facile and single-step hydrothermal	6 M KOH	824 F g <sup>-1</sup> at 4 A g <sup>-1</sup>	-0.1 to 0.4 V	[161]
35.	g-C <sub>3</sub> N <sub>4</sub> /α-Fe <sub>2</sub> O <sub>3</sub>	Solvothermal	2.5 M Li <sub>2</sub> SO <sub>4</sub>	167 F g <sup>-1</sup> at 1 A g <sup>-1</sup>	-1.0 to 0 V	[176]
36.	g-C <sub>3</sub> N <sub>4</sub> @G	Hydrothermal reduction	0.1 M LiClO <sub>4</sub>	264 F g <sup>-1</sup> at 0.4 A g <sup>-1</sup>	0 to 1 V	[177]
37.	g-C <sub>3</sub> N <sub>4</sub> /NiS	Thermal oxidation	6 M KOH	1162 F g <sup>-1</sup> at 1 A g <sup>-1</sup>	0 to 0.6 V	[179]
38.	NiCo <sub>2</sub> O <sub>4</sub> /g-C <sub>3</sub> N <sub>4</sub>	Hydrothermal	6 M KOH	253 F g <sup>-1</sup> at 2 A g <sup>-1</sup>	0 to 0.5 V	[180]
39.	K/Na doped g-C <sub>3</sub> N <sub>4</sub> @MnO <sub>2</sub>	Hydrothermal	1 M Na <sub>2</sub> SO <sub>4</sub>	373.5 F g <sup>-1</sup> at 0.2 A g <sup>-1</sup>	-0.2 to 0.6 V	[181]
40.	Tubular graphitic-C <sub>3</sub> N <sub>4</sub>	Direct slurry casting	6 M KOH	233 F g <sup>-1</sup> at 0.2 A g <sup>-1</sup>	-0.2 to 1.0 V	[182]
41.	C <sub>3</sub> N <sub>4</sub>	Urea pyrolysis	1 M LiClO <sub>4</sub>	113.7 F g <sup>-1</sup> at 0.2 A g <sup>-1</sup>	0.2 to 0.8 V	[183]

combining organic and inorganic electrodes, advanced hybrid electrodes for flexible energy storage could be created, which exhibited high intrinsic chemical reactivity and superior structural stability [110]. The PEDOT shell acts as a protective layer to retain the VN electrode's architecture stable and limit the side reactions on its surface. Apart from having greater surface area, enhanced structural stability and large number of reaction sites, the flexible VN/PEDOT arrays possessed enhanced energy (48.36 Wh kg<sup>-1</sup> at 2 A g<sup>-1</sup>) and power densities (4 kW kg<sup>-1</sup> at 5 A g<sup>-1</sup>).

Lucio-Porto et al. [111] prepared different thicknesses of VN thin films by reactive magnetron sputtering. The VN crystalline films grew in the direction of the plane (111). They also investigated the outcome of varying thicknesses of the electrode material on the electrochemical performance of the as synthesized VN films. It was found that KOH electrolyte offered fast and

reversible redox reactions that tend to pseudocapacitive behavior, while NEt<sub>4</sub>BF<sub>4</sub> in acetonitrile enabled only electric double layer capacitance (EDLC). Fast electron transport was facilitated by the inner core of the VN, in the case of KOH electrolyte. The reaction in Eq. (2) was proposed to elucidate the chemical process.



VN<sub>x</sub>O<sub>y</sub>|OH<sup>-</sup> signifies the EDLC process occurrence, and VN<sub>x</sub>O<sub>y</sub>OH is associated with the compound's reduction of pre-existed vanadium cations. Fig. 4(a) presents the CV curves of VN in different electrolytes (0.5 M KOH, 1 M KOH, and 1 M NEt<sub>4</sub>BF<sub>4</sub>). The CVs

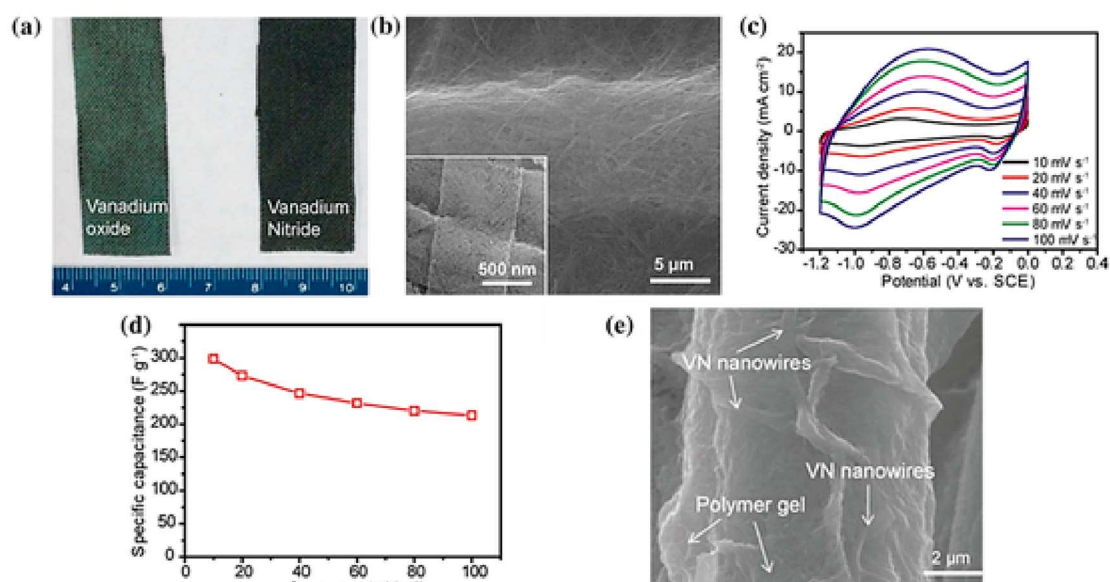


**Fig. 3.** (a) Images of  $\text{VO}_x$  and VN nanowires coated carbon cloth. SEM images of (b) VN nanowires surface view with high magnification in the inset. Electrochemical study of VN nanowire: (c) CV curves, (d) specific capacitance collected at various scan rates. (e) SEM micrograph of VN nanowire embedded in  $\text{LiCl}/\text{PVA}$  gel electrolyte after testing for 10,000 cycles. Reprinted with permission of Liu et al.

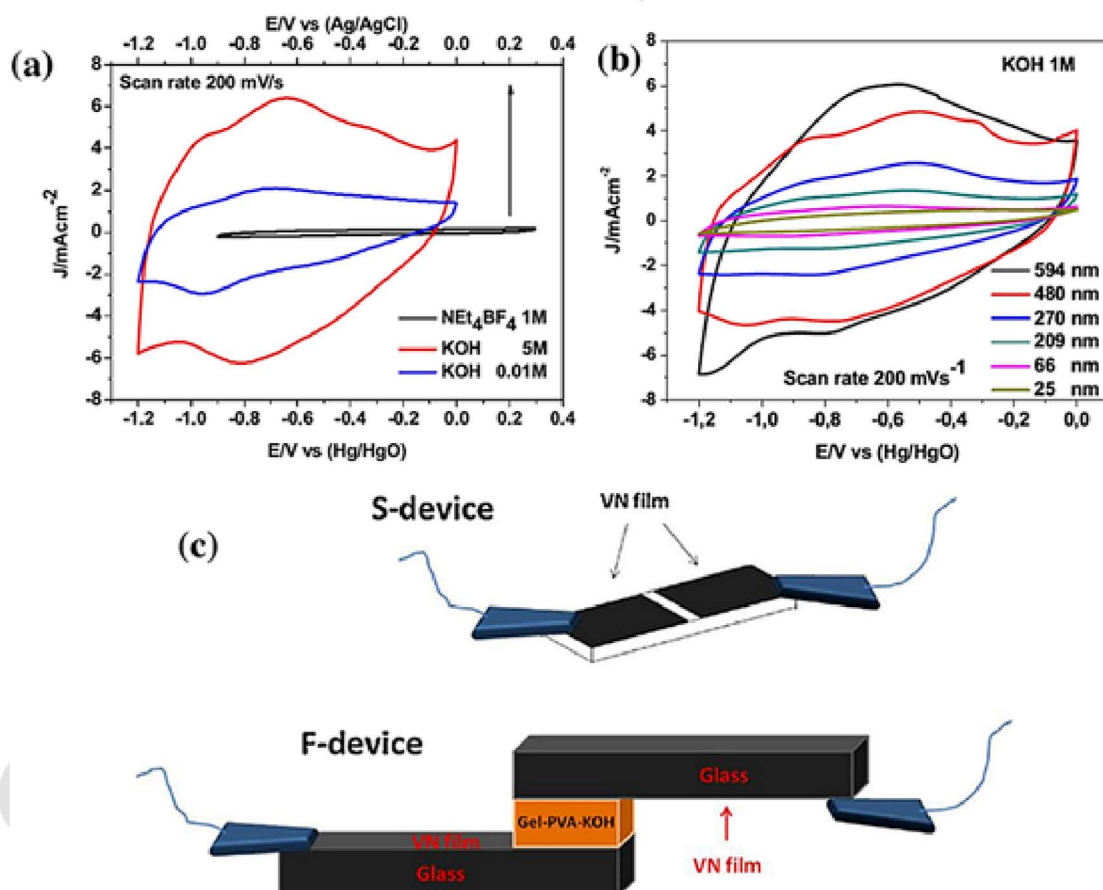


**Fig. 4.** Cyclic voltammetry curves acquired at a scan rate of  $200 \text{ mV s}^{-1}$  of a 480 nm-thick VN film electrode in (a) different concentrations of electrolyte (0.01 M KOH, 5 M KOH, and 1 M  $\text{NET}_4\text{BF}_4$ ), (b) 1 M KOH electrolyte for different VN film thicknesses (25 to 594 nm), and (c) schematic view of two different configurations of contrived supercapacitors, S- and F-devices. Reprinted with permission of Lucio-Porto et al.

were performed on samples of different thicknesses, i.e., 66 and 25 nm, and compared in Fig. 4(b). The redox peaks/waves disappeared in the sample with a thickness of 25 nm; however, a broader peak was observed for the 66 nm-thick VN sample. This demon-

strates the resistive behavior of the 25 nm-thick sample, as VN works simultaneously as an electrochemically-active electrode and current collector. For the 25 nm-thick sample, either the low thickness led to a drop in conductivity, preventing electron transfer

across the electroactive surface, or most of the film thickness was affected by oxidation during the electrochemical cycling, implying the absence of a current collector that limits the amount of electron transfer. This stipulates that samples with a thickness of >25 nm could work as active electrode material as well as conducting medium for electron transfer from the electrode/electrolyte interface. This research implies that the critical thickness of VN thin film was 60 nm, and below this, the performance of VN thin film was not suitable enough to be used for energy storage. In order to prepare a symmetric device, a cutting tool was used to remove a 0.1 cm thin straight line of VN across the glass-coated thin film surface. This gives two VN electrodes on the same glass substrate, marked as Sdevice. A flat S-device with an area of 0.45 cm<sup>2</sup> was selected, and the thin cavity was filled with 1 M KOH electrolyte. Alternatively, an F-device was formed by placing two electrodes face-to-face separated by PVA/KOH solid polymer-electrolyte. Fig. 4(c) shows a drawing of the two kinds of devices. S- and F-devices were assembled to develop a symmetric supercapacitor; both configurations exhibited the same volumetric energy density and capacitance. Sdevice configuration could be used to design micro-devices, as it offers the same capacitive performance as the conventional symmetric supercapacitor design.

Wu et al. reported a new facile multiphase polymeric method for fabricating hybrid VN/carbon composite (VN/C) material for supercapacitor electrodes, consisting of uniformly distributed nanoparticles of VN inside the 3D network of hierarchical porous-carbon. The VN/C electrode demonstrated a greater specific capacitance value of 392 F g<sup>-1</sup> at a current density 0.5 A g<sup>-1</sup> and outstanding rate capability with 50 % capacitance retention even at a very high current density of 30 A g<sup>-1</sup>. TEM image confirmed the presence of small VN quantum dots evenly embedded in the porous carbon. As a result, the carbon matrix acts both as an active material for charge storage and prevents VN aggregation. The electrochemical results revealed that VN/C (vanadyl acetylacetonate/multi-phase polymeric membranes) could be a promising electrode material for energy storage application [112].

Li et al. prepared OD-in-2D pillared-lamellar hybrid covering VN nanodots intercalated in carbon nanosheets (VNNDs/CNSs) via spatially confined strategy through nitridation of organic-inorganic hybrid PANI/V<sub>2</sub>O<sub>5</sub> nanosheets. The inserted PANI converted into 2D CNSs via confining carbonization and sandwiched layers of V<sub>2</sub>O<sub>5</sub> transformed into 3–5 nm diameter's OD VNNDs, resulting in a OD-in-2D pillared lamellar structure. VNNDs/CNSs electrode recorded a high volumetric capacitance of 1203.60 F cm<sup>-3</sup> at 1.10 A cm<sup>-3</sup> and better capacitive stability, superior to electrode based on carbon, transition metal oxides or nitrides. Moreover, this VNNDs/CNSs electrode featured a long cyclic life and capacitance retention of 90 % even after 10,000 electrochemical cycles. These VNNDs (diameter of 3–5 nm) offered plentiful electroactive sites for electrochemical reactions, while the 2D

CNSs acted as an encapsulant that prevented aggregation of the VNNDs and mitigated the dissolution of VN during charging cycles, providing higher capacity and longer cycle life. This approach demonstrated how high volumetric capacitance electrode materials could be designed in a compact, robust, long-lasting and highly conductive manner [64].

Govindarajan et al. investigated Cr-enriched VN thin films as electrode materials for supercapacitors. The pristine VN films as well as VN doped with different Cr concentrations were fabricated using reactive magnetron co-sputtering. Electrodes prepared with these films were investigated directly without any additional binders. The VN doped with 5.7 at.% of Cr exhibited an astonishing capacitive performance with an areal capacitance of 190 mF cm<sup>-2</sup> at a scan rate of 10 mV s<sup>-1</sup>, which is higher compared to the pristine VN (27 mF cm<sup>-2</sup>). Incorporating metals like Cr into metal nitrides could improve their conductivity, especially in supercapacitors [113].

Adalati et al. synthesized VN electrodes using reactive DC magnetron sputtering on 304 stainless steel current collector. Electrodes based on VN thin films had superhydrophilic properties and offered outstanding capacitive performance as well as high capacitance values. Fig. 5(a) depicts the SEM top surface and cross-sectional views of VN thin-film, which revealed 519 nm thick film with triangular nanoflakes. Fig. 5(b) shows the contact angles of the active VN electrode using deionized water (DW) and desired electrolyte, i.e. Na<sub>2</sub>SO<sub>4</sub>. The values of contact angle for water and Na<sub>2</sub>SO<sub>4</sub> on VN electrode were 68° and 26°, respectively. This confirms the hydrophilic nature of VN electrodes for the DW and superior hydrophilic behavior for Na<sub>2</sub>SO<sub>4</sub> electrolyte. These VN active electrodes, operated in the -0.7–0 V potential range, offered an exceptionally greater specific capacitance 229 F g<sup>-1</sup> at 0.50 mA cm<sup>-1</sup> [114].

## 2.2. Chromium nitride (CrN)

As an electrode material for supercapacitors, chromium nitride (CrN) has been extensively studied. The wide band gap and better mechanical and chemical stability of the CrN electrode make it an attractive candidate for supercapacitors.

Adalati et al. designed a flexible electrode by incorporating Pt into Cr<sub>2</sub>N thin film via reactive DC magnetron sputtering. Due to its geometric effect, Pt enhanced electron and ion conductivity as well as the surface area; thus, it delivers greater capacitance and rate capability. The electrochemical measurements of the pure Cr<sub>2</sub>N and Pt-Cr<sub>2</sub>N were acquired in a 1 M Na<sub>2</sub>SO<sub>4</sub> electrolyte, in a potential range from 0 V to +1.1 V. Pt-Cr<sub>2</sub>N offered a high specific capacitance value of 557.0 F g<sup>-1</sup> at 1.0 mA cm<sup>-2</sup>, two-fold higher than the value obtained for pure Cr<sub>2</sub>N (207 F g<sup>-1</sup> at 1.0 mA cm<sup>-1</sup>). Fig. 6(a, b) depicts the CV (at

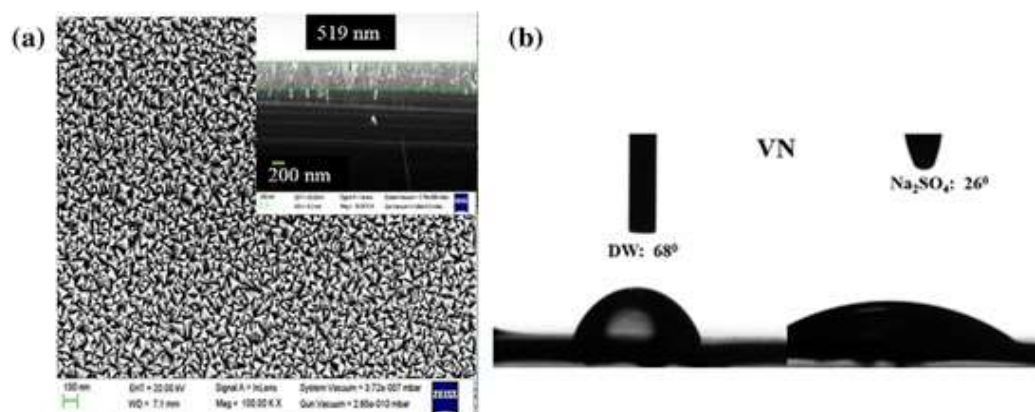
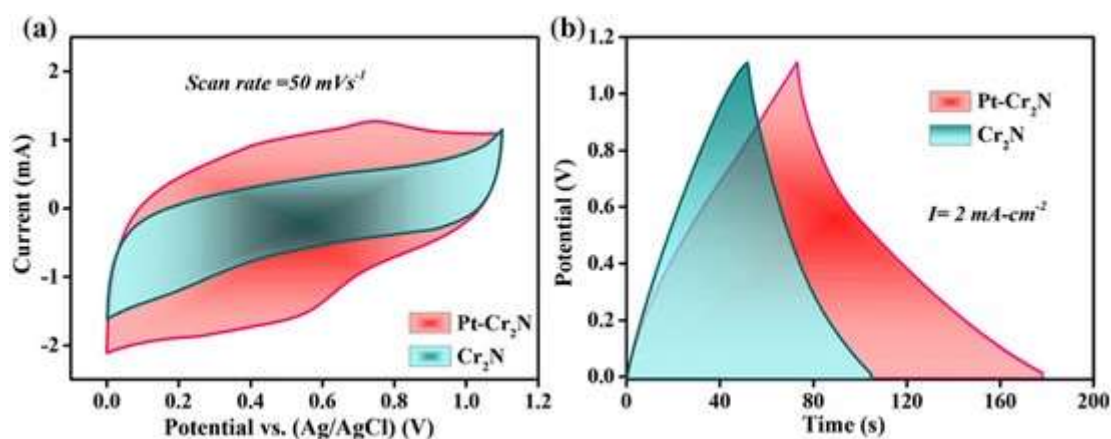


Fig. 5. (a) Top view FE-SEM and cross-section view (inset) of VN electrode, and (b) wetting property (contact angle) of VN electrode surface measured in DI water and Na<sub>2</sub>SO<sub>4</sub> aqueous solution. Reprinted with permission of Adalati et al.





**Fig. 6.** Electrochemical property of sputtered grown Cr<sub>2</sub>N and Pt-Cr<sub>2</sub>N composite electrodes to visualize the enhanced performance upon Pt insertion: (a) CV curves at the scan rate of 50 mV s<sup>-1</sup>, and (b) GCD curves at 2 mA cm<sup>-2</sup>. Reprinted with permission of Adalati et al.

50 mV s<sup>-1</sup>) and GCD (at 2.0 mA cm<sup>-1</sup>) curves of Cr<sub>2</sub>N and Pt-Cr<sub>2</sub>N electrodes to visualize the enhanced integrated area of the peak current, ultimately pointing towards enhanced capacitance value [115].

Zhang et al. prepared a hollow Cr<sub>2</sub>O<sub>3</sub>/CrN nanoshell in ammonium atmosphere. Cr<sub>2</sub>O<sub>3</sub> powder in alumina boat, heated up to 750 °C at a ramp rate of 10 °C min<sup>-1</sup> under continuous flow of NH<sub>3</sub> gas, gradually turned into CrN and, after some time of ammoniation, unreacted NH<sub>3</sub> was removed and Cr<sub>2</sub>O<sub>3</sub>/CrN nanoshell remained as the final product. In Cr<sub>2</sub>O<sub>3</sub>/CrN composites, the electrochemical performance of Cr<sub>2</sub>O<sub>3</sub> was improved by inserting crystalline and high conductive CrN. Cr<sub>2</sub>O<sub>3</sub>/CrN composites displayed higher specific capacitance of 333.2 F g<sup>-1</sup> at a scan rate of 10 mV s<sup>-1</sup>, and preserved about 84.7 % of the initial capacitance value even after 5000 electrochemical cycles, owing to the maximum specific surface area and stable crystal structure of the electrode [116].

Nanostructured CrN porous films were deposited by oblique angle sputtering by Qi et al. to assemble a symmetric supercapacitor. The CrN demonstrated better areal capacitance value of 17.7 mF cm<sup>-2</sup> at 1.0 mA cm<sup>-2</sup>. Furthermore, the nanostructured porous CrN thin film based symmetric supercapacitor exhibited good electrochemical performance and delivered high volumetric energy density and power density of 7.4 mWh cm<sup>-3</sup> and 18.2 mW cm<sup>-3</sup>, respectively at 2.0 mA cm<sup>-2</sup> [117].

Free-standing 3D CrN@nitrogen-doped carbon nanosheet arrays were prepared by sputtering technique on carbon paper (CrN@NCs@CP) and assessed as an electrode material for a supercapacitor, proposed by Xu et al. Fig. 7(a, b) depicts the SEM view micrographs of the CrN@NCs@CP electrode surface. SEM image reveal that the CrN@NCs uniformly coat and inclined above the carbon paper surface. The average thickness of the CrN@NCs was roughly 360 nm, and the copious space between neighboring CrN@NCs stimulated electrolyte diffusion. The CrN@NCs@CP electrode exhibited enhanced capacitive performance, and acquired a high areal capacitance of 132.1 mF cm<sup>-2</sup> at 1.0 mA cm<sup>-2</sup> along with a long cyclability and a capacitance retention of 95.9 % after 20,000 electrochemical cycles. The capacitive performances of different types of NCs@CP, CrN@CP, and CrN@NCs@CP electrode materials were assessed and their comparison revealed that CrN@NCs@CP was the most performing electrode for supercapacitor; the electrochemical characteristics of the electrodes are presented in Fig. 7(c, d). The CrN@NCs@CP electrode showed higher areal capacitance compared to CrN@CP electrode (4.1 mF cm<sup>-2</sup> at 1.0 mA cm<sup>-2</sup>). The GCD curves of CrN@NCs@CP and bare CrN@CP electrodes displayed a symmetric triangular shape, which implies that the charge storage mechanism was governed by both double-layer capacitance and pseudocapacitance, as summarized in the Eq. (3) below.



where CrN-H<sup>+</sup> and CrN || H<sup>+</sup> stand respectively for the double layer capacitance and pseudo-capacitance charge storage [118].

### 2.3. Cobalt nitride (CoN)

Cobalt nitride displays exceptional physical properties just like an interstitial metallic compound and a stable binary nitride of a 3d metal system. Cobalt-based framework has metal-like properties, as nitrogen atoms incorporated on interstitial sites form covalent bonding with cobalt atoms. These metal like properties are expected to confer cobalt nitride with better electrochemical properties [119].

In order to produce highly efficient supercapacitors, Zhang et al. developed a free-standing binder-free Co<sub>3</sub>N thin film using reactive magnetron sputtering at varying deposition times: T1 (10 min), T2 (20 min), T3 (30 min), and T4 (40 min). These samples were optimized to achieve higher porosity level as a function of deposition time. Fig. 8 (a-d) depicts the SEM micrographs of the electrodes T1-T4, allowing to visualize the porosity of the thin film surface. A granular structure dispersed throughout the substrate surface was obvious for all the samples. Out of all the samples, T3 had larger grain size and offered better electrochemical performance. Electrochemical analysis of T1-T4 electrodes is presented in Fig. 9(a-c). Among the thin film electrodes, T3 electrode reached a maximum charge capacity of 47.5 mC cm<sup>-2</sup> at 1.0 mA cm<sup>-2</sup> and a capacitance retention of 78.1 % post 10,000 electrochemical cycles [120].

Liu et al. designed nickel-cobalt alloys and their nitrides (Ni-doped Co-Co<sub>2</sub>N) with controlled nanostructure features for high performing electrode material. This Ni-doped Co-Co<sub>2</sub>N was synthesized by simple thermal annealing of metal-organic framework (MOF)-derived NiCo<sub>2</sub>O<sub>4</sub> in ammonium atmosphere at 350 °C. The final product retained the MOF-derived two-dimensional (2D) nanoflake arrays and consisted of metal-metal nitride heterostructure. Metal nitride incorporated with metal nanoparticles provided improved electrical conductivity along with controlled nanocrystallinity and uniform distribution. Ni-doped Co-Co<sub>2</sub>N electrode delivered a specific capacity of 361.93C g<sup>-1</sup> at 2 mA cm<sup>-2</sup> and good rate capability; it retained 57.37 % of the capacitance when the current density was raised from 2 to 50 mA cm<sup>-2</sup> [121].

Adalati et al. prepared crystalline and catalyst-free CoN electrodes using a single step method on a flexible SS-304 (stainless steel) current collector for high-efficiency supercapacitors. In 1 M Na<sub>2</sub>SO<sub>4</sub> aqueous electrolyte, CoN electrode exhibited high capacitive performance and excellent cyclic life due to its high mechanical strength, electrochemical stability, and tremendous electrical conductivity (low resistivity of approximately 10<sup>-3</sup> to 10<sup>-4</sup> Ω cm at RT). CoN electrode operated in a volt-

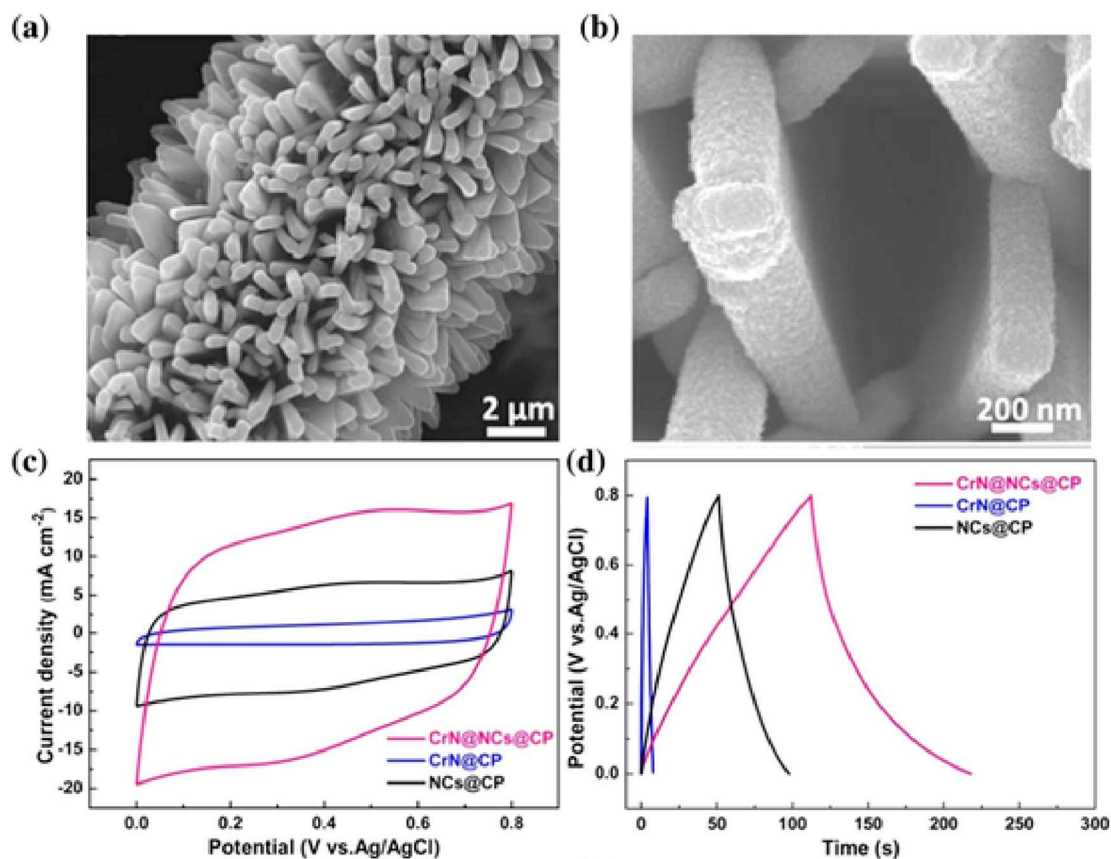


Fig. 7. SEM top-view images at low (a) and high (b) magnifications of CrN@NCs@CP. Electrochemical properties of the prepared NCs@CP, CrN@CP, and CrN@NCs@CP electrodes: (c) CV, and (d) GCD curves. Reprinted with permission of Xu et al.

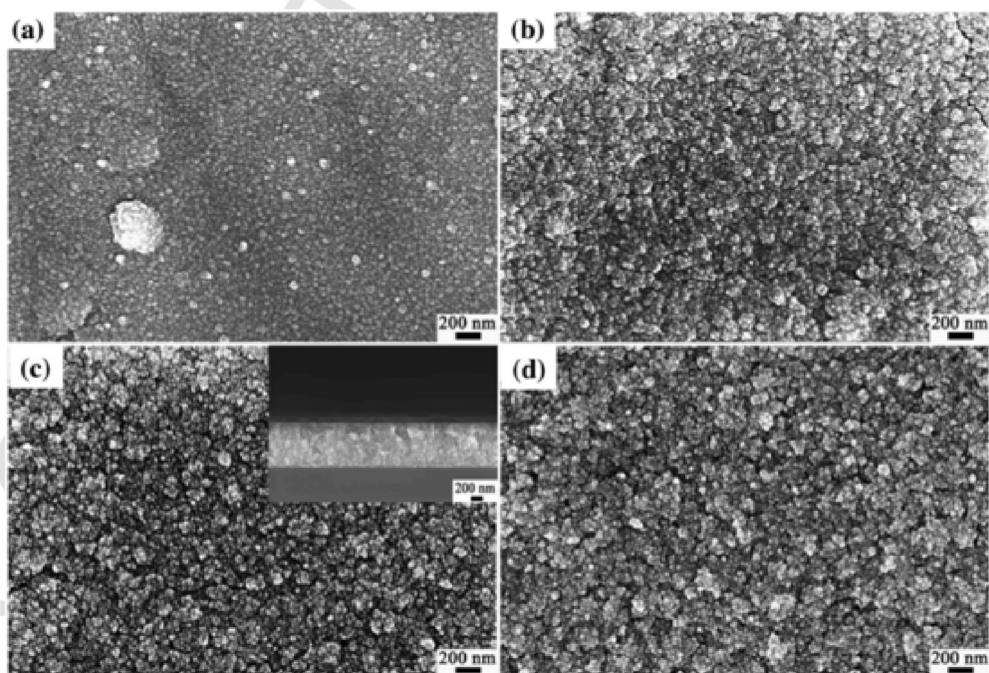
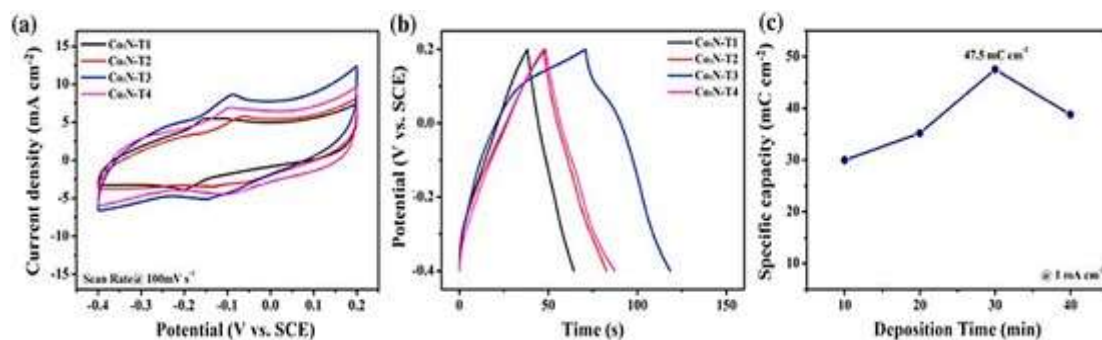


Fig. 8. SEM surface morphology of sputter-grown CoN thin film electrodes for different deposition times: (a) T1 (10 min), (b) T2 (20 min), (c) T3 (10 min) with cross section view in inset, and (d) T4 (40 min). Reprinted with permission of Zhang et al.

age window from  $-1.0$  to  $0.0$  V and achieved a high  $520 \text{ F g}^{-1}$  capacitance value at a current density of  $0.50 \text{ mA cm}^{-2}$ . Additionally, an asymmetric supercapacitor (ASC) was developed by employing CoN as negative and  $\text{Zn}_3\text{N}_2$  as positive electrodes. The ASC could operate in a



**Fig. 9.** Electrochemical properties of T1-T4 CoN thin film electrodes: (a) CV curves at 100 mV s<sup>-1</sup> scan rate, (b) GCD curves, and (c) comparison of the specific capacity at 1.0 mA cm<sup>-2</sup>. Reprinted with permission of Zhang et al.

broad voltage range (2 V) and offered good capacitance value of 75.4 F g<sup>-1</sup> along with high energy density 42 Wh kg<sup>-1</sup> (optimum power density of 3.123 kW kg<sup>-1</sup>) at 0.5 mA cm<sup>-2</sup> [122].

#### 2.4. Tungsten nitride (WN)

Tungsten nitride (WN) is one of the least studied transition metal nitrides as an electrode material, despite its greater electrical conductivity. Though, some of the research available on WN-based electrodes revealed excellent electrochemical performance to contrive supercapacitor devices.

In addition to its application in the plating of diffusion barriers, high-K dielectric materials, supercapacitor electrodes, Li-ion battery electrodes, and nucleation layers, atomic layer deposition (ALD) is a promising method for the synthesis of WN [65]. Nandi et al. [123] reported the synthesis of h-W<sub>2</sub>N by ALD with 0.35 Å per ALD cycle growth rate within a narrow temperature window of 180–195 °C, using tungsten hexacarbonyl and ammonia as precursors [124].

To combine the interesting capacitance value and greater electric conductivity, Ouendi et al. [125] deposited tungsten nitride (W<sub>2</sub>N) thin films on Si<sub>3</sub>N<sub>4</sub> coated silicon (Si) substrate by using sputtering technique. Comparing the performance of the films synthesized at different temperatures, the sample produced at room temperature acquired the best electrochemical results. This sputtered W<sub>2</sub>N film (7.9 μm thick) revealed exceptional electrochemical properties and offered high areal (550 mF cm<sup>-2</sup>) and volumetric capacitances (>700 F cm<sup>-3</sup>) at a scan rate of 5 mV s<sup>-1</sup> in 1 M KOH electrolyte.

Prakash et al. [126] developed W<sub>2</sub>N binder-free electrodes on stainless-steel substrates using sputtering method for effective supercapacitors. In their experiments, they found that the fabricated W<sub>2</sub>N thin films recorded a good specific capacitance value of 163 F g<sup>-1</sup> at 0.5 mA cm<sup>-2</sup> and proved to be a good choice for long life span device with a 90.46 % capacity retention after 10,000 electrochemical cycles.

Salman et al. produced WN-rGOF and WO<sub>3</sub>-rGOF hybrid fiber electrodes for high-performing flexible supercapacitors. Integration of WN in rGOF (graphene oxide fibers) enhanced the conductivity and electrochemical property of WN-rGOF, which possessed 7.5- and 1.75-times higher capacitance compared to rGOF and WO<sub>3</sub>-rGOF electrodes, respectively, and offered a capacitance of 16.29 F cm<sup>-3</sup> and an energy density of 1.448 mW h cm<sup>-3</sup> at 0.05 A cm<sup>-2</sup>. Fig. 10(a) illustrates the SEM cross-section image WN-rGOF, revealing the formation of fibers. WN insertion in rGOF enhanced the conductivity of the final composite (WN-rGOF), which was higher compared to that of WO<sub>3</sub>-rGOF, presented in Fig. 10(b). CV and GCD curves acquired for WN-rGOF, WO<sub>3</sub>-rGOF and rGOF are depicted in Fig. 10(c & d), and clearly evidenced the higher capacitive performance of WN-rGOF compared to WO<sub>3</sub>-rGOF and rGOF [127].

#### 2.5. Manganese nitride (Mn—N)

Mn N binary system exists in four stable intermediate phases, the face-centered cubic structure of Mn<sub>4</sub>N, hexagonal structure of Mn<sub>2</sub>N, and tetragonal structure of Mn<sub>3</sub>N<sub>2</sub> and MnN. These Mn N phases possess metallic behavior, which functions as a conductive layer between the surface of the catalyst and electrode, offering faster charge transfer, favorable for exceptional electrochemical applications [103,128].

Durai et al. [129] reported binder-free manganese nitride (Mn<sub>3</sub>N<sub>2</sub>) electrode prepared by the sputtering technique. FE-SEM analysis in Fig. 11(a) revealed that Mn<sub>3</sub>N<sub>2</sub> particles were in the nanoscale range with a pyramidal shape and uniformly covering the full surface of the substrate. In this study, the effect of different electrolytes (1 M KOH, 1 M KCl and 1 M Na<sub>2</sub>SO<sub>4</sub>) was investigated. The highest areal capacitance of Mn<sub>3</sub>N<sub>2</sub> electrode was recorded in KOH (118 mF cm<sup>-2</sup> at 10 mV s<sup>-1</sup>), while for KCl and Na<sub>2</sub>SO<sub>4</sub>, capacitance values of 68 and 27 mF cm<sup>-2</sup> were achieved, respectively at a scan rate 10 mV s<sup>-1</sup>. Fig. 11(b) depicts the rate capability of the electrode in the different electrolytes. Mn<sub>3</sub>N<sub>2</sub> electrodes demonstrated marvellous cyclability with a capacitance retention of 98.5 % in 1 M KOH, 89 % in 1 M KCl, and 83 % in 1 M Na<sub>2</sub>SO<sub>4</sub>, after 4000 electrochemical cycles.

Sridhar et al. [93] synthesized manganese nitride decorated on reduced graphene oxide substrate (MnN@rGO) by using microwave nitridation technique for high performance sodium ion batteries, supercapacitors and EMI shielding applications. When utilized as a sodium anode ion battery, the synthesized nanostructure showed excellent performance with significant sodium storage capacity of 716 mAhg<sup>-1</sup> even after 180 cycles demonstrating the powerful interaction between reduced graphene and nanoparticles of MnN with the substrate. Further, MnN@rGO nanocomposites exhibited good supercapacitive performance with high capacitance of 639.2 F g<sup>-1</sup> in 1 M aqueous electrolyte of Na<sub>2</sub>SO<sub>4</sub> at a scan rate of 10 mV s<sup>-1</sup>. The efficiency of the EMI shielding about 30 dB was measured in the 2–18 GHz of X-band area.

Zhang et al. [130] synthesized intermetallic MnN by nitriding MnO<sub>2</sub> in an environment of NH<sub>3</sub> at 800 °C. The MnN electrode exhibited a maximum volumetric capacitance of 1044.3 F cm<sup>-3</sup> at a current density of 1 A g<sup>-1</sup> in 1 M Na<sub>2</sub>SO<sub>4</sub> (aq), and <1 % of the capacitance was lost after 5000 ladder cycles. At a current density of 10 Ag<sup>-1</sup>, 89.3 % of the initial volumetric capacitance was still retained. Long cycle life was provided by a reversible electrode process controlled by diffusion and a high electrical conductivity during charging-discharging. For particle applications, MnN/Na<sub>2</sub>SO<sub>4</sub>/MnN symmetrical capacitor was assembled and displayed exhibits a high volumetric energy density of 112.2 W h L<sup>-1</sup>.

#### 2.6. Titanium nitride (Ti—N)

Titanium nitride (TiN) thin films have been widely used as protective coatings in machinery and contacts in microelectronics due to their exceptional hardness, mechanical stability, biostability, and high elec-



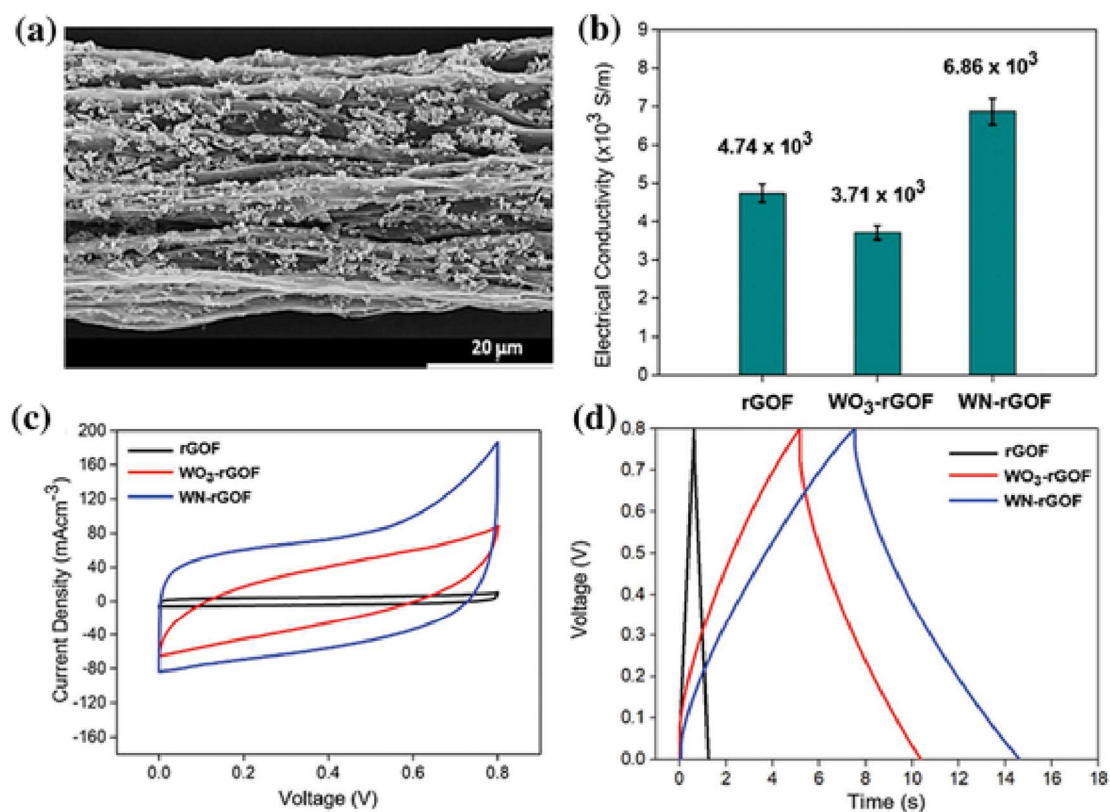


**Fig. 10.** (a) SEM cross-section view of WN-rGOF hybrid fibers. (b) Electrical conductivity comparison of rGOF, WO<sub>3</sub>-rGOF and WN-rGOF. Electrochemical performance of the supercapacitors based on WN-rGOF, WO<sub>3</sub>-rGOF and rGOF: (c) CV curves at 10 mV s<sup>-1</sup>, and (d) GCD curves at 0.05 A cm<sup>-2</sup>. Reprinted with permission of Salman et al.

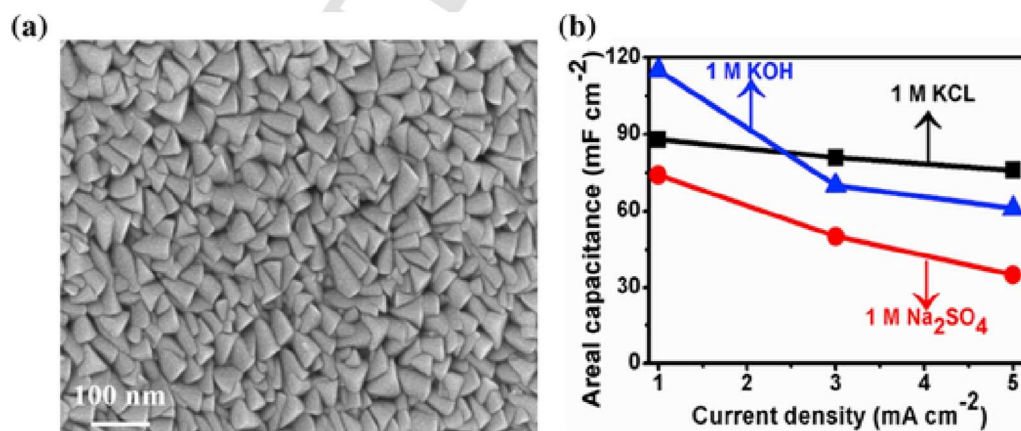


**Fig. 11.** (a) FE-SEM image of Mn<sub>3</sub>N<sub>2</sub> thin film electrode, and (b) its electrochemical performance in different electrolyte solutions. Reprinted with permission of Durai

trical conductivity ( $4 \times 10^3$  to  $5.55 \times 10^4$  S cm<sup>-1</sup>). Increased oxygen vacancies of the native oxide in TiN films and low relaxation time constant ( $\delta_0$ ) for discharge have also led to usages in electrochemical supercapacitors for increased capacitance [8,88,131,132].

Sun et al. [132] prepared porous titanium nitride (TiN) electrode films on silicon substrate by sputtering and studied the working pressure influence on the physico-chemical properties of TiN films electrode. The electrochemical performance of the electrode was tested in 1 M KCl electrolyte. This study suggests that when deposition pressure increased from 0.3 to 1.3 Pa, a significant improvement occurred in areal capacitance and value increased from 0.3 to 4.7 mF cm<sup>-2</sup>, at a current density of 0.05 mA cm<sup>-2</sup>. This improvement is ascribed to a larger effective area and more active oxynitride (TiO<sub>x</sub>N<sub>y</sub>) in the films de-

posited at 1.3 Pa pressure. Moreover, the electrode deposited at 1.3 Pa acquired an exceptional cycling stability over 10,000 cycles, which is slightly lower than that deposited at 1.1 Pa working pressure. Further, this group also optimized the best thickness (deposition time) for excellent electrochemical performance.

Achour et al. [88] reported sputter-grown TiN films with controlled porosity and assessed their electrochemical performance dependence on thickness, porosity, and surface chemistry of electrodes. The prepared electrodes were tested electrochemically in 0.5 M K<sub>2</sub>SO<sub>4</sub> and found outstanding cycling stability over 20,000 cycles. A six-fold increase in areal capacitances of the TiN films from 0.68 to 4.25 mF cm<sup>-2</sup> (at 100 mV s<sup>-1</sup>) for T2 (150 W) and T4 (80 W) films, respectively, through optimization of deposition conditions, without sacrificing their



cycling life or power density. This study suggests that using low deposition temperature (<100 °C) for synthesizing TiN electrodes for microsupercapacitor without CNT templates will reduce processing costs and facilitate easy electrode integration due to the simple device structure.

The same group [133] prepared titanium vanadium (TiVN) based binary transition metal nitride thin film electrodes. DC co-sputtering of vanadium (V) and titanium (Ti) targets was used to deposit this binary transition metal nitride. The capacitive performance of TiVN film was studied for different Ti/V atomic ratios to optimize the betterperforming electrode. In the electrochemical study, it was observed that the electrode with larger V content exhibited higher areal capacitance but restricts to limited cyclic life. On the other hand, adding a high amount of Ti leads to better cyclic stability but reduces the areal capacitance of the electrode. This study concludes that a 1.1 Ti/V atomic ratio in electrode promises a higher areal capacitance up to 15 mF cm<sup>-2</sup> with optimum cyclic stability in 1 M KOH electrolyte solution.

Kao et al. [134] reported titanium nitride (TiN) coated carbon nanotube (CNT) forest electrodes by using an atomic layer deposition (ALD) technique for supercapacitors and tested their electrochemical behavior in 0.5 M H<sub>2</sub>SO<sub>4</sub> aqueous solution. ALD provides conformal coatings with angstrom level precision and offers more flexibility in the choice and architecture of the device. Capacitive performance increased by >500 % for TiN-CNT devices compared to bare CNTs, due to increased oxygen vacancies on the TiN surfaces. TiN-CNTs, as compared with bare CNTs and planar TiN, exhibit areal capacitance values of 81 mF cm<sup>-2</sup>, 14 mF cm<sup>-2</sup>, and 0.2 mF cm<sup>-2</sup>, respectively, at a scan rate of 10 mV s<sup>-1</sup>.

Ansari et al. [135] prepared TiN nanoparticles with an average size of 30 nm on the Ti foil by potentiostat electrolysis in KCl solution. This TiN/Ti electrode was tested electrochemically in an acetonitrile solution of 1.0 M LiClO<sub>4</sub>. TiN/Ti electrode exhibited a high capacitance of 53.66 mF cm<sup>-2</sup> at a scan rate of 6.66 mA cm<sup>-2</sup> with only 3 % capacitance loss even after 10,000 cycles.

### 2.7. Molybdenum nitride (MoN)

The rocksalt type  $\gamma$ -MoN<sub>x</sub>, (x is typically comprised between 0.39 and 0.54) is the most studied form of molybdenum nitride, with this other forms also attract attention, such as hexagonal phases  $\delta_1$ -MoN,  $\delta_2$ -MoN, and  $\delta_3$ -MoN with compositions close to stoichiometry and disordered nitrogen vacancies [136–138]. The  $\alpha$ -phase occurs with small amounts of dissolved nitrogen in molybdenum metal, whereas  $\beta$ -Mo<sub>2</sub>N is tetragonal with ordered stacking faults distorted rocksalt-type and necessitates special synthesis conditions [139,140]. On the other hand, Mo<sub>5</sub>N<sub>6</sub> was obtained by Mo<sub>2</sub>S ammonolysis. Molybdenum nitrides received huge attention because of their extraordinary properties, such as catalytic activity for ammonia synthesis, alkane hydrogenolysis and dehydrogenation, hydrodesulfurization, and

hydrodenitrogenation [141, 142]. These properties of MoN have been used in corrosion resistance, superconductivity, wear resistance, electrocatalytic activity in the hydrogen evolution reaction, and diffusion resistance [143]. With these outstanding properties, MoN has been used as electrode material for supercapacitors, owing to its charge storage capability and high electrochemical activity.

Shah et al. [87] conducted the reactions of MoCl<sub>5</sub> or Mo(NMe<sub>2</sub>)<sub>4</sub> with ammonia to synthesize cubic  $\gamma$ -Mo<sub>2</sub>N or hexagonal  $\delta_1$ -MoN depending on reaction temperature and time. Relatively high surface areas are observed in the porous particles of the chloride (MoCl<sub>5</sub>) derived materials and offered high capacitances of 275 F g<sup>-1</sup> (and 202 F g<sup>-1</sup>) at 2 mV s<sup>-1</sup> when electrodes tested in aqueous 0.5 M K<sub>2</sub>SO<sub>4</sub> (and 0.5 M H<sub>2</sub>SO<sub>4</sub>) electrolytes. Despite very low surface areas, imide-derived (Mo(NMe<sub>2</sub>)<sub>4</sub>) samples offer significant amounts of capacitance 161 F g<sup>-1</sup> (and 148 F g<sup>-1</sup>) in an aqueous 0.5 M K<sub>2</sub>SO<sub>4</sub> (and 0.5 M H<sub>2</sub>SO<sub>4</sub>) electrolytes. The samples heated at 600 °C exhibit high specific capacitance, presumably due to the complete decomposition of all amide and organic groups (0 % H). The electrochemical study suggested that MoCl<sub>5</sub>-derived materials exhibit a double layer charging mechanism while those obtained from Mo(NMe<sub>2</sub>)<sub>4</sub> exhibit strong redox features.

Lv et al. [144] prepared a flexible helical structure of MoN modified on nitrogen-doped carbon cloth (CC@CN@MoN) via a simple electrodeposition process for health care application. This electrode was electrochemically tested in 1 M LiOH electrolyte and offered a high areal capacitance of 467.6 mF cm<sup>-2</sup> at a current density of 5 mA cm<sup>-2</sup> with long cycle stability of 10,000 cycles.

Kumar et al. [145] synthesized binary metal nitride nanorods of nickel-molybdenum nitride (Ni<sub>2</sub>Mo<sub>3</sub>N) via a one-pot hydrothermal method and calcination at 400C followed by ammonolysis at 800C. Ni<sub>2</sub>Mo<sub>3</sub>N nanorods are tested as an electrode material for supercapacitors in 6 M KOH and attained a high capacitance value of 264C g<sup>-1</sup> at a current density of 0.5 A g<sup>-1</sup> with 81 % capacitance retention for 1000 charging-discharging cycles.

Yen-Jui et al. [131] developed MoN by facile thermal nitridation of electrodeposited molybdenum oxide and assessed its performance as electrode material in 0.5 M H<sub>2</sub>SO<sub>4</sub> electrolyte for supercapacitor application. The molybdenum oxide electrode showed a normalized capacitance of 0.67 mF cm<sup>-2</sup>, while after nitridation, procured MoN offered enhanced capacitance around 16 mF cm<sup>-2</sup> at a scan rate of 50 mV s<sup>-1</sup>.

### 3. Alkali metals and alkali earth metals: lithium nitride

In the group of alkali metals and alkali earth metals, lithium nitride Li<sub>3</sub>N is the only alkali stable binary nitride. The bonding of nitrogen with alkali metals and alkali earth metals is depicted in Fig. 12(a). Formation energy for other binary nitrides from group 1 element is less favorable, as calculated lattice

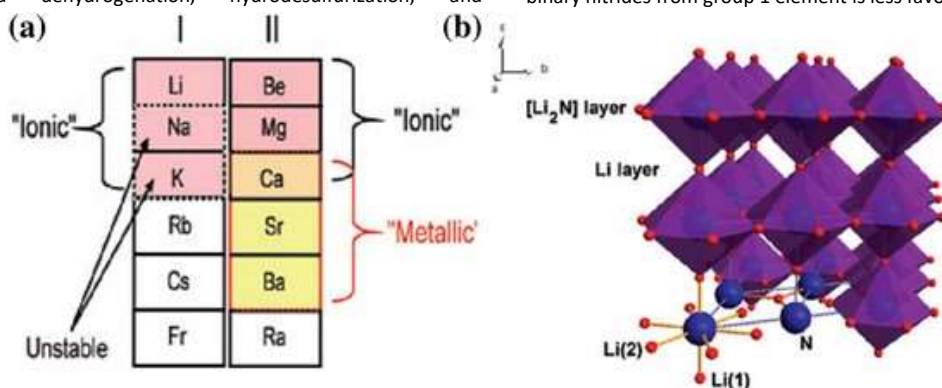


Fig. 12. (a) Stable binary nitrides from periodic groups 1 and 2 and their bonding character. (b) Crystal structure of  $\alpha$ -Li<sub>3</sub>N. Reprinted with permission of Gregory et al.

energy suggests, and other binary nitrides like  $\text{Na}_3\text{N}$  and  $\text{K}_3\text{N}$  require specific conditions to become stable.  $\text{Li}_3\text{N}$  is formed at ambient temperature upon exposure of  $\text{Li}$  to dry nitrogen, as  $\text{Li}_3\text{N}$  has high negative Gibbs-free energy of formation,  $\Delta G_f = -128.64 \text{ kJ mol}^{-1}$ . Out of all three existing forms of  $\text{Li}_3\text{N}$ ,  $\alpha$ -polymorph is stable at ambient pressure and temperature.  $\alpha$ -Form at adequate conditions (4.2 kbar at 300 K) gives rise to  $\beta$ - $\text{Li}_3\text{N}$ , while the  $\gamma$ - $\text{Li}_3\text{N}$  arises from  $\beta$ - $\text{Li}_3\text{N}$  between 35 and 45 GPa and remains stable up to 200 GPa. The  $\alpha$ - $\text{Li}_3\text{N}$  phase occurs in a hexagonal structure, as nitrogen sits at the center of ab-plane in the edge-sharing layers of planar lithium-hexagons (Fig. 12(b)).  $\alpha$ - $\text{Li}_3\text{N}$  with excellent  $\text{Li}^+$  ion mobility is an indirect band-gap semiconductor (2.1 eV) and is known for its exceptionally high  $\text{Li}^+$  ion conduction [146]. However, it was initially proposed that nitrides might be used in lithium secondary batteries because of their low decomposition potential (0.5 V) [147]. Chen et al. [148] used  $\text{N}_2$  plasma activation of  $\text{Li}$  metal to design a multifunctional protective flower shaped and highly [001] oriented  $\text{Li}_3\text{N}$  layer on the  $\text{Li}$  metal surface by using plasma activation for <5 min.  $\text{Li}_3\text{N}$  layer possessed good ionic conductivity ( $5.02 \times 10^{-1} \text{ mS cm}^{-1}$ ) and high Young's modulus of 48 GPa. Prior to use, MTI corporation's  $\text{Li}$  chips (450  $\mu\text{m}$  thick) were cleaned with sharp blades until they were shiny. A properly sealed vessel was used to place the  $\text{Li}$  chips from the Ar glove box to the quartz tube, as shown

in Fig. 13(a). While observing the surface morphology through SEM at higher magnification, the surface of bare  $\text{Li}$  was relatively smooth. At higher magnification, some pits and defects were observed, as demonstrated in Fig. 13(b). These pits act as nuclei causing uneven deposition of  $\text{Li}$  and lead to the formation of dendrites during the plating of  $\text{Li}$  [149]. This causes the formation of  $\text{Li}_3\text{N}$  flower shaped cluster on  $\text{Li}$  metal after the plasma treatment. Fig. 13(c, e) depicts the SEM micrographs of the samples prepared for different plasma activation times (1, 2 and 3 min). The time of  $\text{N}_2$  plasma exposure affects the growth of the  $\text{Li}_3\text{N}$  layer. As exposure time increased, a dense flower shape layer evolved on the top of the  $\text{Li}$  metal surface. According to the island-growth mechanism,  $\text{Li}_3\text{N}$  first grows at the defect spots to form the nucleus and then expands into two dimensions and produces a dense  $\text{Li}_3\text{N}$  layer. This process could be used to fabricate nanostructured  $\text{Li}_3\text{N}$  layer for excellent electrochemical energy storage. Copper substitution in  $\text{Li}_3\text{N}$  showed notable effect on ionic conductivity. Limited replacement of  $\text{Li}$  by  $\text{Cu}$  in  $\text{Li}_3\text{N}$  materials reduced the  $\text{Li}$  vacancies (charge carriers) within the nitride, as recommended by early research works on  $\text{Li}_3\text{N}$  [150]. A number of electrochemical studies demonstrated that copper, nickel, and iron ternary nitrides performed extremely well as electrodes over multiple charge-discharge cycles for electrochemical reactions [151].

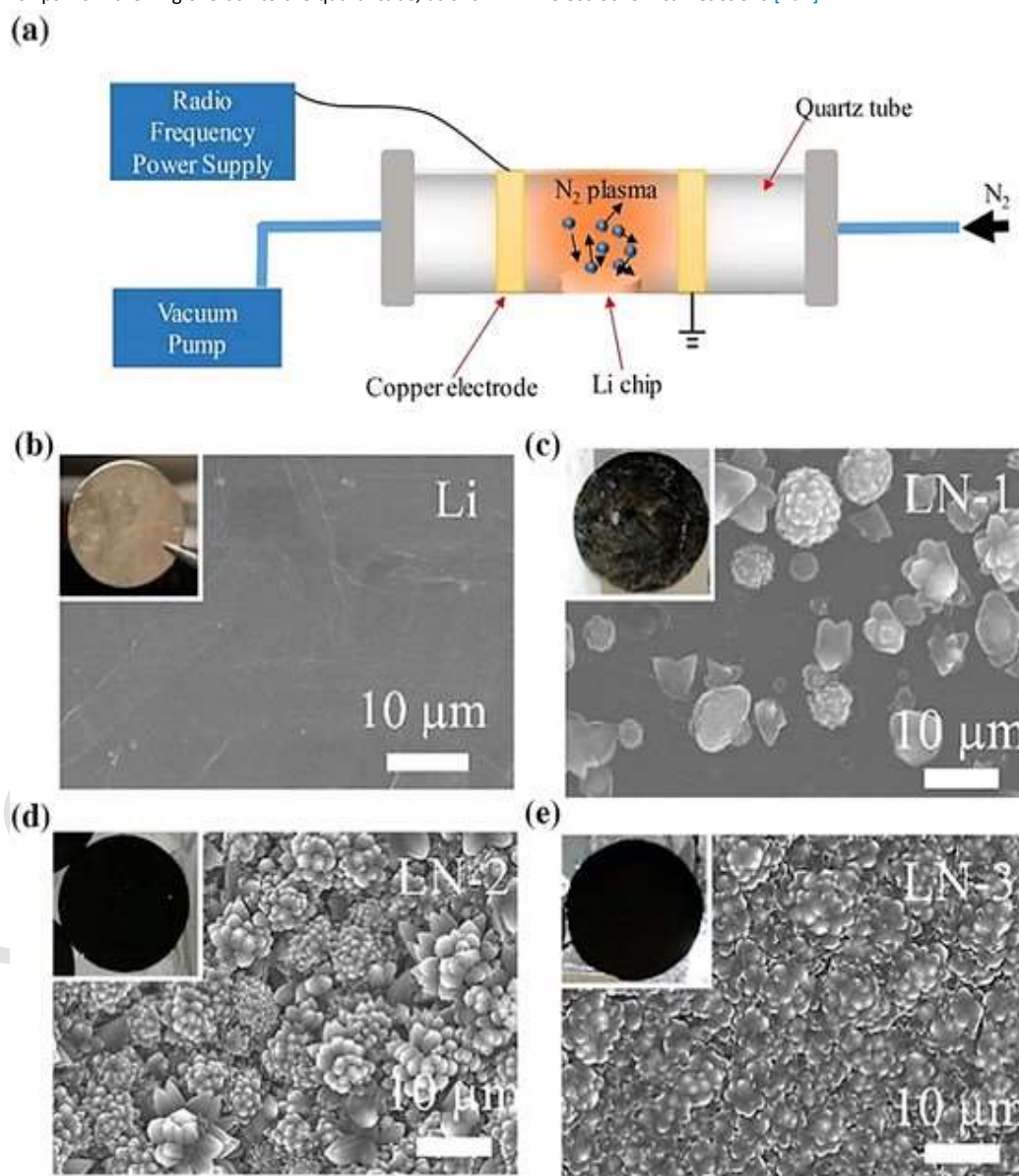


Fig. 13. (a) Experimental setup for the synthesis of  $\text{Li}_3\text{N}$  film electrode and SEM micrographs with the corresponding photos (in inset) of  $\text{Li}_3\text{N}$  films at varying times of  $\text{N}_2$  plasma exposure. (b) Bare  $\text{Li}$ , (c) 1-min, (d) 2-min, and (e) 3-min plasma activation processing. Reprinted with permission of Chen et al.

Tapia-Ruiz et al. reported that one of the few stable binary compounds, formed by an alkali metal and nitrogen, Li—N, is an ideal material for energy storage applications and involves the transportation of lithium ions for energy applications. By relying on structural analogies between boron nitride and hexagonal graphene, they showed that alkali group elements and nitrogen can also be used to form such low dimensional structures. One and two-dimensional Li<sub>3</sub>N nanostructures, despite the lack of an equivalent van der Waals gap, could be grown. In nanostructured form, Li ion diffusion was enhanced compared to the bulk compound, promising materials with remarkable ionic mobility [152].

Xie et al. stated that by burning a mixture of graphene and LiNO<sub>3</sub>, composites of graphene and LiNO<sub>3</sub> (GLs) can be fabricated. GLs were tested electrochemically as supercapacitor electrode materials and revealed exceptional capacitive performance and acquired greater specific capacitance value of 3339.7 F g<sup>-1</sup> at 1 mV s<sup>-1</sup> and 80.07 F g<sup>-1</sup> at 20 A g<sup>-1</sup> and outstanding stability. Fig. 14(a) displays the CV curves of GLs acquired at several scan rates. The CV of the GLs exhibited obvious redox peaks, that might be attributed to the redox of Li<sup>+</sup> complexed on the surface of graphene, and which could result in the redox capacitance during measurement. Upon increasing the scan rate, the GLs electrode showed better capabilities and excellent capacity retention, as presented in Fig. 14(b). GLs electrode displayed high cyclic stability, retained 83.32 % capacitance even after 7000 electrochemical cycles at 20 A g<sup>-1</sup> [153].

Using *N,N*-dimethylformamide (DMF) to homogenize electrode slurry, Liu et al. prepared a Li<sub>3</sub>N-containing electrode for the first time using a commercially viable route. The soft package lithium-ion capacitor was formed by mixing only 12 wt% Li<sub>3</sub>N in activated carbon electrode (AC- Li<sub>3</sub>N) and demonstrated outstanding rate capability, cyclic stability and superb capacity. AC-Li<sub>3</sub>N (370 mAh g<sup>-1</sup>) recorded 2.3 times-higher capacity than Li<sub>3</sub>N-free AC (90 mAh g<sup>-1</sup>) at 14 mA g<sup>-1</sup>. AC- Li<sub>3</sub>N retained 90 % of its capacitance after 10,000 cycles [154].

#### 4. Icosagens: boron nitride (BN)

Recently, 2D materials like graphene have been extensively used to advance research on supercapacitor electrodes. However, graphene sheets re-stacking property reduces its active surface area, making it unsuitable for capacitor applications [155]. Therefore, the fabrication of electrode materials for supercapacitors is focused on graphene analogs such as boron nitride (BN). BN belongs to the class of 2D materials exhibiting unique properties [156]. BN has outstanding thermal conductivity, high mechanical strength, excellent dielectric properties, and exhibits atomically smooth surfaces. Since pure BN electrodes are insulating (electronic bandgap of 4–6 eV), they cannot be used in energy storage. For this reason, doping or heterostructure processes

involving other materials are necessary to make BN a potential candidate. Doping processes introduce free electrons, which enhance charge carrier mobility, leading to higher intrinsic electrochemical activity [157]. As a result of the slight difference between B and C atoms' electro-negativities, polar covalent bonds (B-C) are formed in the h-BN-graphene composite as validated by Kumar et al., enhancing the BN electrode's electrochemical performance for energy storage [158]. The occurrence of two different chemical species (B & N) in the sub-lattices of h-BN and inversion symmetry of the graphene help in developing electrochemically-active h-BN/graphene composites [159].

Maity et al. demonstrated that composite materials of functionalized BNs and CNTs, as well as polyaniline (PANI), are useful materials for supercapacitor electrodes. Functionalization of BN was successfully achieved using KMnO<sub>4</sub> (m<sub>K</sub>-BN) and hydrogen peroxide (m<sub>H</sub>-BN), and investigated for their potential to enhance electrochemical activity and serve as electrodes for supercapacitors. Fig. 15(a, b) depicts CV and GCD plots of composite materials consisting of functionalized BN electrodes (m<sub>K</sub>-BN/CNT/PANI, m<sub>H</sub>-BN/CNT/PANI, and m<sub>K</sub>-BN/CNT). In the working potential window of 0 to 0.8 V and using 1 M KCl as electrolyte, m<sub>K</sub>-BN/CNT/PANI possessed enhanced surface area and showed the highest specific capacitance 515 F g<sup>-1</sup> compared to m<sub>H</sub>-BN/CNT/PANI (417 F g<sup>-1</sup>) at 1 A g<sup>-1</sup> [160].

A facile and straightforward hydrothermal method was reported by Saha et al. for the preparation of h-BN/rGO hybrid nanostructures. Fig. 16(a–d) presents the FE-SEM images of the prepared samples for various rGO concentrations named as BNO (pure BN), BNG1 (0.1 g rGO), BNG2 (0.15 g rGO), and BNG3 (0.2 g rGO). Increased rGO content in the composite successfully reduced the band gap of the insulator h-BN. rGO decreased the solution resistance as well as the charge transfer resistance of h-BN, increasing its electrical conductivity and enabling better ion exchange. In 6 M KOH aqueous electrolyte, the electrochemical performance was evaluated for all prepared samples with varying levels of rGO concentrations, as depicted in Fig. 16(e, f) [161]. When the rGO content (atomic concentration) was carefully controlled in the h-BN, the composite (BNG2) provided a specific capacitance of 824 F g<sup>-1</sup> at 4 A g<sup>-1</sup>, while BNG0, BNG1, and BNG3 offered lower specific capacitances of 182.2, 384 and 720 F g<sup>-1</sup>, respectively, at the same current density.

#### 5. Crystallogens: carbon nitride

Carbon materials have been extensively applied as electrodes for EDLCs due to their good electrical conductivity, large specific surface area, and electrochemical stability. Carbon materials such as porous carbon and graphene are potential candidates for supercapacitor elec-

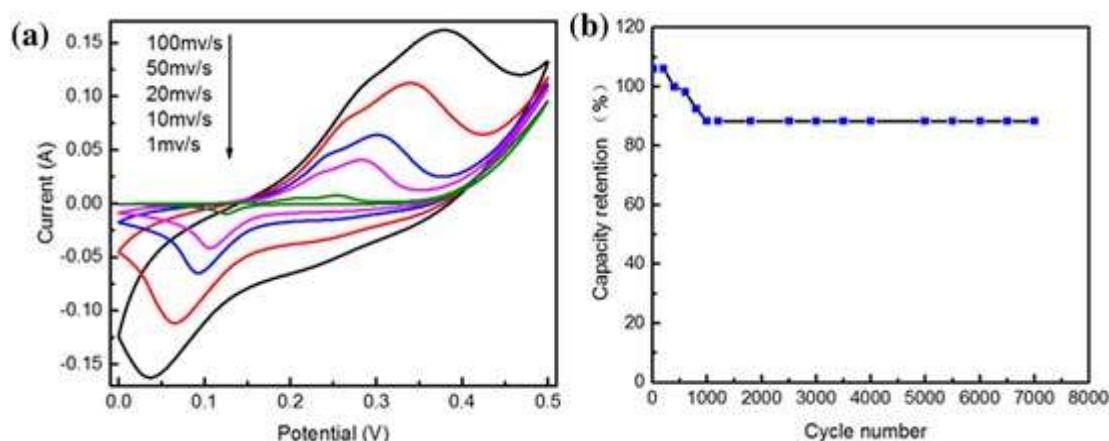


**Fig. 14.** Electrochemical properties of GLs electrode (graphene-LiNO<sub>3</sub> composite): (a) CV curves at various scan rates, and (b) capacity retention after 8000 electrochemical cycles at 20 A g<sup>-1</sup>. Reprinted with permission of Xie et al.

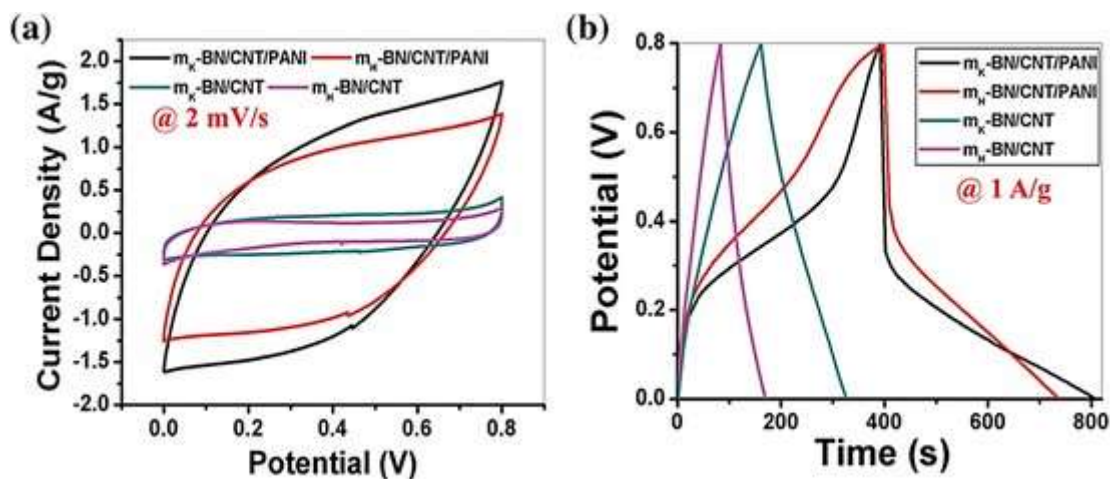


**Fig. 15.** Electrochemical performance of the  $m_K$ -BN/CNT/PANI,  $m_H$ -BN/CNT/PANI,  $m_K$ -BN/CNT, and  $m_H$ -BN/CNT composite electrodes: (a) CV curves recorded at a scan rate of 2 mV s<sup>-1</sup>, and (b) GCD plots acquired at 1 A g<sup>-1</sup>. Reprinted with permission of Maity et al.

trodes [162–167]. Recently another form of carbon, graphitic carbon nitride (g-C<sub>3</sub>N<sub>4</sub>), attracted attention of researchers with the aim to combine the excellent properties of carbon and nitrogen for electrochemical energy storage applications. The unique electronic properties of g-C<sub>3</sub>N<sub>4</sub> and its convenient preparation have encouraged its application as an electrode material for supercapacitors [168–172]. High content of nitrogen in g-C<sub>3</sub>N<sub>4</sub> could offer plentiful of active-sites for redox reactions. Furthermore, g-C<sub>3</sub>N<sub>4</sub> has a large theoretical surface area, stable structure, and composition similar to that of graphene [173,174]. However, due to serious stacking of g-C<sub>3</sub>N<sub>4</sub> sheets, research is mainly focused on its composites with other capacitive materials [175].

Xu et al. reported a composite of g-C<sub>3</sub>N<sub>4</sub> and  $\alpha$ -Fe<sub>2</sub>O<sub>3</sub> prepared via ionic liquid-assisted method; the composite featured a specific capacitance of 167 F g<sup>-1</sup> at 1 A g<sup>-1</sup> in 2.5 M Li<sub>2</sub>SO<sub>4</sub> electrolyte [176]. Chen's group functionalized graphene with g-C<sub>3</sub>N<sub>4</sub>; the resulting composite recorded a good specific capacitance of 264 F g<sup>-1</sup> at a current density of 1 A g<sup>-1</sup> in 0.4 M LiClO<sub>4</sub> electrolyte [177].

Li et al. synthesized a pseudo-capacitive g-C<sub>3</sub>N<sub>4</sub>/NiCo<sub>2</sub>S<sub>4</sub> composite with outstanding electrochemical stability and a high capacitance value of 1557 F g<sup>-1</sup> at 1 A g<sup>-1</sup>. g-C<sub>3</sub>N<sub>4</sub> has the characteristics of N-doped materials with enhanced electron transport rate and increased surface wettability [178].

Sun et al. [179] obtained TC-g-C<sub>3</sub>N<sub>4</sub> by oxidation exfoliation of BC-g-C<sub>3</sub>N<sub>4</sub>, which delivered the prerequisite for the NiS particles to fully settle inside and on the surface of the carbon nitride. During this process of insertion of NiS in TC-g-C<sub>3</sub>N<sub>4</sub> and BC-g-C<sub>3</sub>N<sub>4</sub>, NiS particles were uniformly formed on g-C<sub>3</sub>N<sub>4</sub> layers, Fig. 17(a). In comparison with the performance of pristine g-C<sub>3</sub>N<sub>4</sub> and NiS, TC-g-C<sub>3</sub>N<sub>4</sub>/NiS active electrode material retained high pseudo-capacitance over 8000 cycles (1162 F g<sup>-1</sup> at a current density of 1 A g<sup>-1</sup>) and exhibited outstanding cycle stability (capacitance retention of 82 % after 8000 electrochemical cycles). The electrochemical performance of the as-prepared electrodes were assessed by GCD at a current density of 1 A g<sup>-1</sup> and CV at the 10 mV s<sup>-1</sup> scan rate, Fig. 17(b & c). Pristine g-C<sub>3</sub>N<sub>4</sub> electrode discharged in only about 10 s (GCD curve) and had a small integral area of CV curves, which indicates its negligible electrochemical properties compared to all other composites (TC-g-C<sub>3</sub>N<sub>4</sub> and BC-g-C<sub>3</sub>N<sub>4</sub>), suggesting that the modification of g-C<sub>3</sub>N<sub>4</sub> is essential to achieve better electrochemical performance.

Guan et al. discussed the morphology effect of NiCo<sub>2</sub>O<sub>4</sub> nanostructures loaded onto C<sub>3</sub>N<sub>4</sub> sheets on the capacitive performance. Nickel and cobalt chlorides were used as precursors in thiourea pyrolysis for 3 h at 550 °C to synthesize the NiCo<sub>2</sub>O<sub>4</sub> and C<sub>3</sub>N<sub>4</sub> composites. Fig. 18(a) displays the SEM micrographs of different NiCo<sub>2</sub>O<sub>4</sub>-g-C<sub>3</sub>N<sub>4</sub> composites: NNC-I (nanosheets) and NNC-II (nanoneedles). Using two different methods, NNC-I was prepared with

oil bath, and NNC-II was synthesized hydrothermally. Electrochemical results suggested that NNC-II had high capacitance of 274.8 F g<sup>-1</sup> at 1 A g<sup>-1</sup> and a retention rate of 101 % post 1000 electrochemical-cycles at a current density of 4 A g<sup>-1</sup>, see Fig. 18(b), while NNC-I recorded a specific capacitance of only 182.2 F g<sup>-1</sup> at the same current density [180].

Shan et al. reported electrochemical study of Na or K single atoms doped C<sub>3</sub>N<sub>4</sub>. The electrochemical results revealed that the Na- and K-doped C<sub>3</sub>N<sub>4</sub> achieved high values of capacitance (374.0 and 295.0 F g<sup>-1</sup>, respectively at a current density of 0.2 A g<sup>-1</sup>) compared to the non-doped one (96.0 F g<sup>-1</sup> at a current density of 0.2 A g<sup>-1</sup>). Capacitance retentions were 59.10 % for the non-doped, 93.70 % for the Na-doped and 95.2 % for the K-doped material, after 1000 electrochemical cycles at a current density of 1 A g<sup>-1</sup> [181].

Tahir et al. [182] fabricated tubular structures of C<sub>3</sub>N<sub>4</sub> using melamine as a precursor with capacitance values of 233.0 and 204.0 F g<sup>-1</sup> at 0.20 and 0.5 A g<sup>-1</sup>, respectively. The tubular nanostructured C<sub>3</sub>N<sub>4</sub> exhibited good capacitance retention (90.9 % and 89.2 % at respectively at 0.2 and 0.50 A g<sup>-1</sup>) after 1000 electrochemical cycles. The results were also compared with those of bulk C<sub>3</sub>N<sub>4</sub> developed under similar settings, which revealed poor performance compared to the nanostructured form.

Gonçalves et al. discussed the electrochemical behavior of C<sub>3</sub>N<sub>4</sub> electrodes, produced by urea pyrolysis route (casting), to understand the essential characteristics of bare C<sub>3</sub>N<sub>4</sub> for supercapacitor electrode. The C<sub>3</sub>N<sub>4</sub> electrode acquired a specific capacitance of 113.70 F g<sup>-1</sup> at a current density of 0.20 A g<sup>-1</sup> with a capacitance retention of 89.20 % after 5000 electrochemical cycles. Fig. 19(a & b) depicts the CV and GCD curves before and after 5000 cycles of charging-discharging [183]. The CV curve retained the same shape even after 5000 electrochemical cycles with a slight decline in peak current. In the GCD profiles, the first and last GCD cycles took 20.6 s and 16.5 s for discharging, respectively; the small change in discharging time led to a slight decrease in the capacitance.

## 6. Conclusion and future outlooks

Electrochemical energy storage is widely explored using metal nitrides with inherent novel properties. A comprehensive review of the current state-of-the-art in metal nitride research is presented in this article, including electronic structure manipulation, morphological structure design, and electrochemical energy storage applications. This review is focused on recent progress on stable binary metal nitrides. These metal nitrides are suitable and represent potential candidates for supercapacitor electrodes as they possess exceptional properties such as



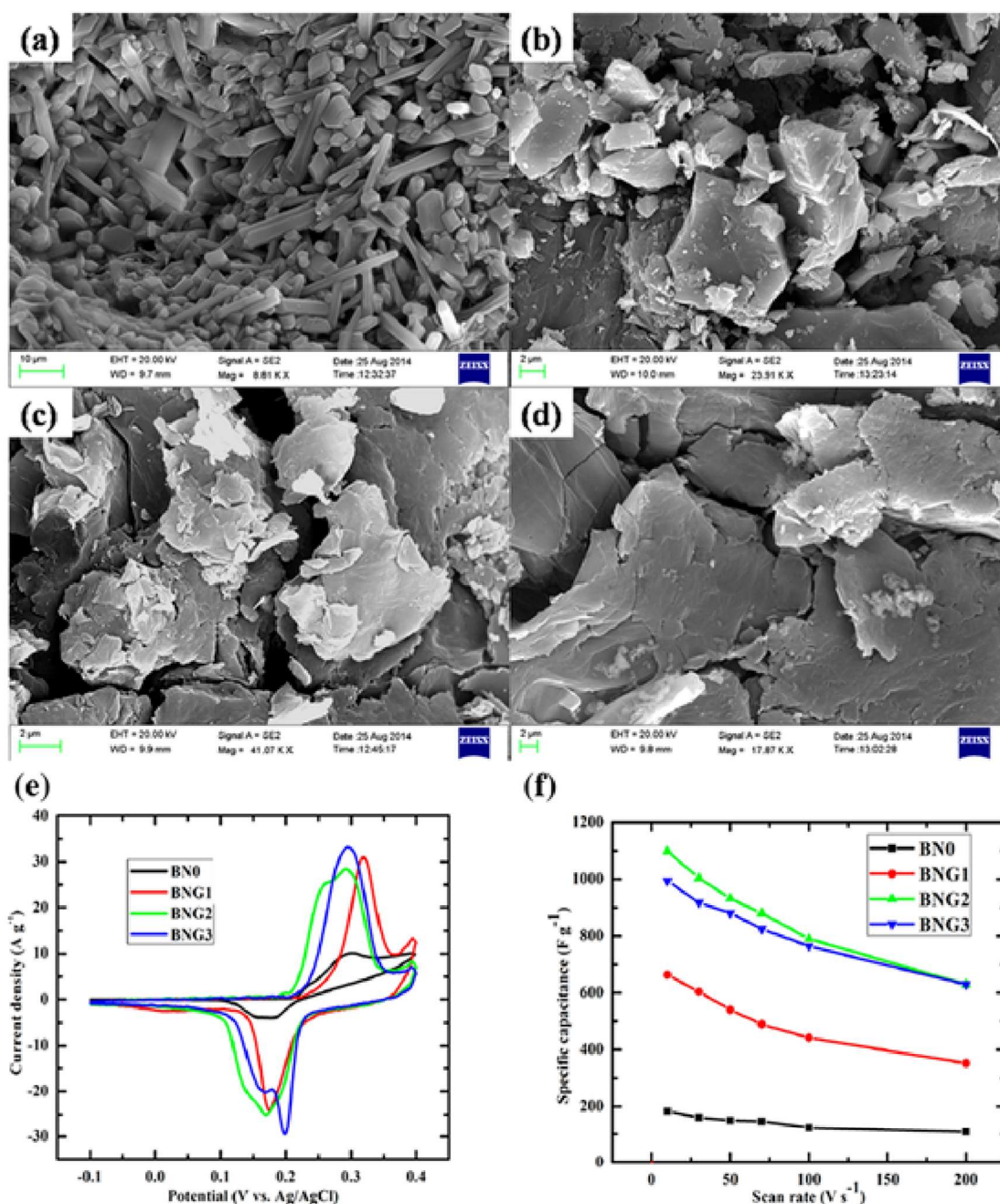


**Fig. 16.** FE-SEM images of (a) BNO, (b) BNG1, (c) BNG2, and (d) BNG3; (e) CV plots at  $10 \text{ mV s}^{-1}$  scan rate, and (f) variation of the specific capacitance with scan rate. Reprinted with permission of Saha et al.

high electrical conductivity, exceptional theoretical capacitance, good electrochemical stability, and high thermal stability. However, elements of the different periodic table groups own varying properties, as metal bonding with nitrogen depends on the parent group of metal. These bonding variations occur due to the electronegativity difference between parent metal and nitrogen, which is metal dependent. According to the bonding strength of metal and nitrogen in the formed metal nitride, the final stable binary nitride possesses unique properties that can be utilized in energy storage applications. Furthermore, several energy storage devices can be designed to fully harness the quality of metal nitrides, such as electrochemical capacitors, asymmetric, solid-state, and flexible supercapacitors. Metal nitride-based electrochemical energy storage devices can also be used with other energy collecting devices such as solar and thermoelectric cells in an electronic circuit to form integrated systems. Metal nitrides with high mechanical strength

and corrosion resistance properties can be used as body-embedded electrodes for any electronic device. This idea of implanting metal nitride electrodes as body cover/panel will provide extended shelf-life for electronic devices. Most metal nitrides show ductile behavior, which is ideal for bending performance. Electrodes with ductile nature are an excellent selection for flexible energy storage cells to use in real-life flexible electronic devices. In this context, the following points should stress the research directions in metal nitride materials.

- (i) **Synthesis method:** Multifunctional platforms can be built from nanosized metal nitrides. Predictably, there will be many more solutions in the future, especially in the energy sector. Metal nitrides can be synthesized in several ways. Ammonia reduction annealing is the primary technique for the preparation of nitrides. Metal nitrides with different morphologies can be

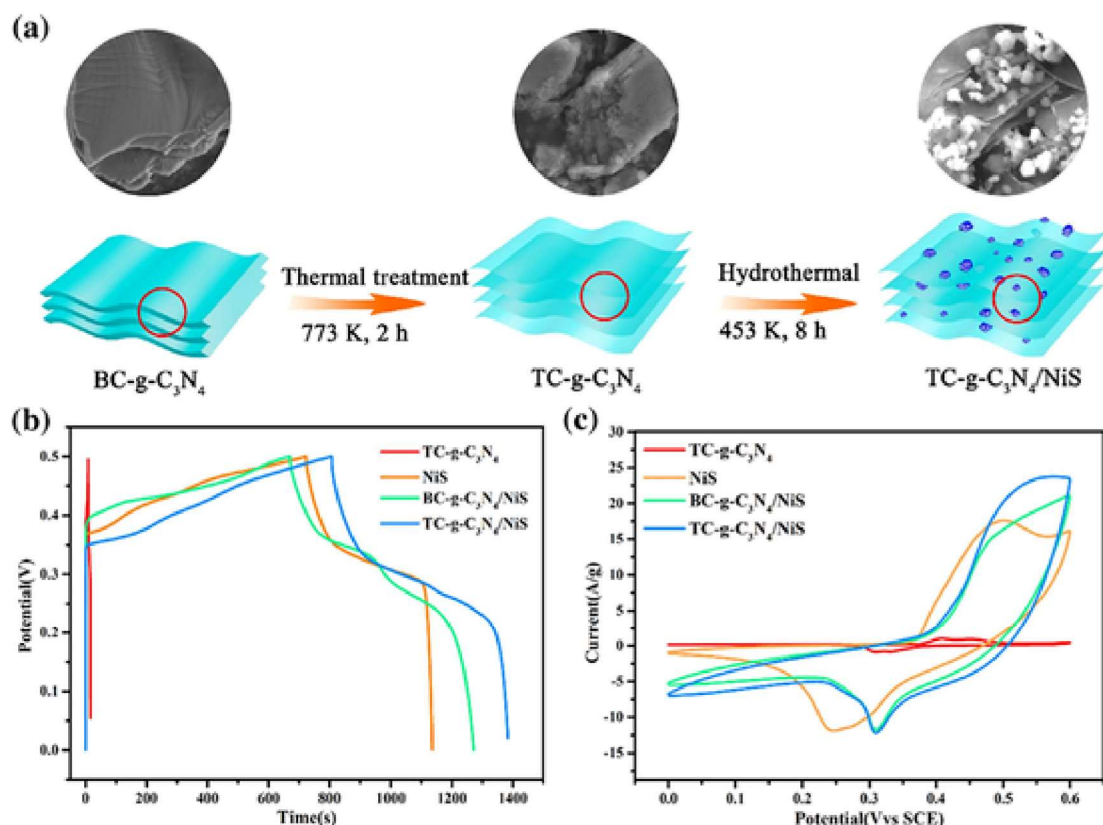


Fig. 17. (a) Schematic view of the preparation processes of TC-g-C<sub>3</sub>N<sub>4</sub> and TC-g-C<sub>3</sub>N<sub>4</sub>/NiS. Electrochemical properties of B-g-C<sub>3</sub>N<sub>4</sub>, BC-g-C<sub>3</sub>N<sub>4</sub>, T-g-C<sub>3</sub>N<sub>4</sub>, and TC-g-C<sub>3</sub>N<sub>4</sub>: (b) GCD curves at 1 A g<sup>-1</sup>, and (c) CV plots at 10 mV s<sup>-1</sup> scan rate. Reprinted with permission of Sun et al.

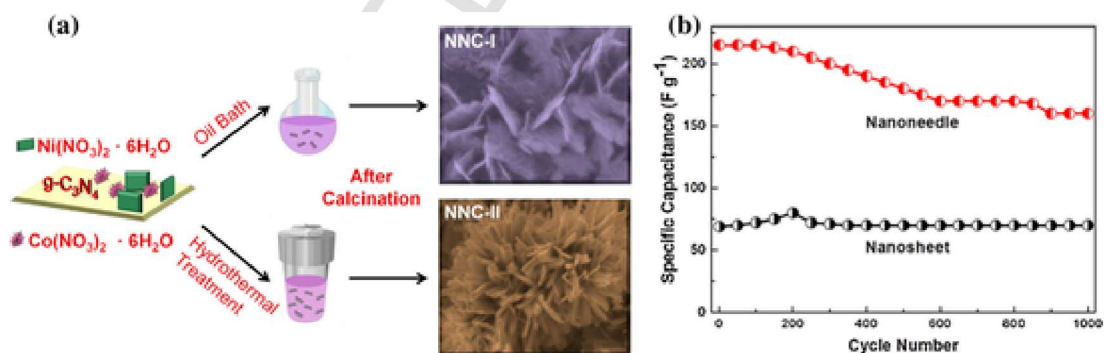


Fig. 18. (a) Schematic view of the synthetic process and possible formation mechanism of g-C<sub>3</sub>N<sub>4</sub> different nanostructures: NNC-I (nanosheets) and NNC-II (nanoneedles), (b) variation of the capacitance with cycle number at a current density of 4 A g<sup>-1</sup> of NNC-I and NNC-II. Reprinted with permission of Guan et al.

synthesized using the hydrothermal method depending on heating time. However, this method is unsuitable for preparing metal nitride films because these films are not uniform in thickness. Sputtered films are generally used for this since their thickness is uniform, but the films' capacitance may be low because of their compactness.

- (ii) Composite materials: Due to the synergistic effects of the individual components, forming combinations of nitrogen with various metals is a flexible and effective technology. These effects primarily relate to the rapid characterization of electron/ion transfer, the prevention of the decomposition of active material, the provision of additional pseudocapacitance, the creation of more active sites, the prevention of the aggregation of nanoparticles, and the collapse of microstructure. Nitrides have been extensively explored in association with carbon-based materials, metals, or other heteroatoms of metals and metal oxides. Finding the ideal molar ratio of each composition is

another important task in performance majorization. In addition to investigating hybrid materials with various combinations, it should be noted that certain underlying negative impacts may surface throughout the preparation process.

- (iii) Exploring new metal nitrides. According to current development, the nitride materials for electrochemical supercapacitors mainly focus on W, V, Mn, Co, Cr, B, and C nitrides in the metal nitride family. Since some nitrides, such as pure BN electrodes, are insulating (electronic bandgap of 4–6 eV), they cannot be used in energy storage. For this reason, doping or heterostructure processes involving other materials are necessary to make BN a potential candidate, and the emphasis of further research will be on exploring new composition of BN and metal nitrides. Recently another form of carbon, graphitic carbon nitride (g-C<sub>3</sub>N<sub>4</sub>), attracted the attention of researchers intending to combine the excellent properties of carbon and nitrogen for electrochemical energy storage applications.



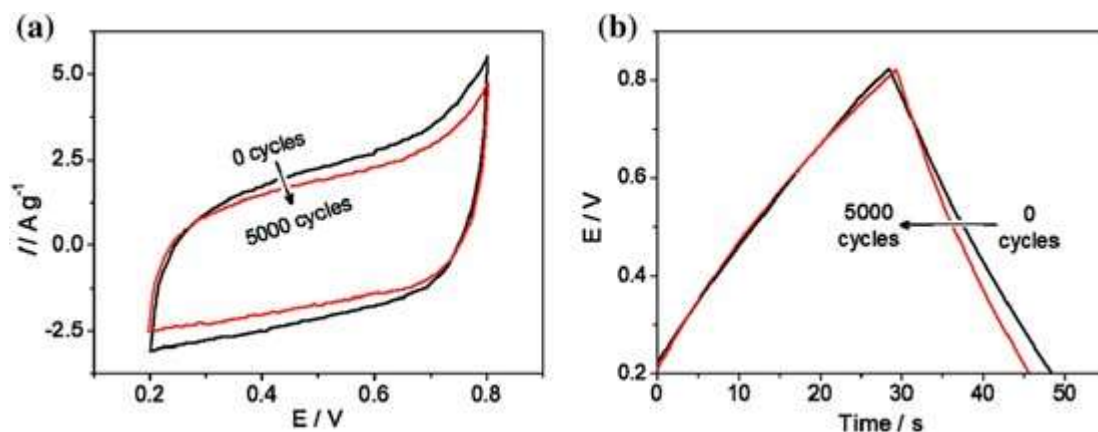


Fig. 19. Cyclic stability test of  $C_3N_4$  electrode for 5000 electrochemical cycles: (a) CV at  $80 \text{ mA s}^{-1}$ , and (b) GCD at a current density of  $3.0 \text{ A g}^{-1}$ . Reprinted with permission of Gonçalves et al.

The unique electronic properties of g- $C_3N_4$  and its convenient preparation have encouraged its application as an electrode material for supercapacitors.

(iv) Choosing proper electrolytes. The electrolytes that are employed, as well as the intrinsic features of the electrode materials, affect the potential range of supercapacitors. Due to the evolution of hydrogen and oxygen, the potential window in an aqueous electrolyte is restricted; in contrast, an ionic liquid medium can enable the possibility of a larger output voltage. The advantages of safety and leak-tightness make anhydrous polymer gel electrolytes the preferred choice for building solid-state energy storage systems. The electrode and electrolyte must be appropriately combined as part of its ideal operating environment to maximize the electrochemical performance.

These outcomes of metal nitride-based electrodes confirm that metal nitrides represent an interesting topic for researchers and can be selected as a possible candidate for supercapacitor electrodes. This review offers insight for the researchers to select an element from the periodic table to develop a metal nitride electrode and deliberate all aspects of the electrochemical supercapacitor to improve the electrochemical performance. **Declaration of competing interest**

The authors declare that they have no known competing financial interests or personal relationships that could have appeared to influence the work reported in this paper.

#### Data availability

The authors do not have permission to share data.

#### Acknowledgments

Ravikant Adalati one of the author acknowledges financial support from CSIR, New Delhi (Grant No. 09/143 (0912)/2018-EMR-I). Dr. Rabah Boukherroub thanks the ANR for financial support of the project "SIREVIVAL" of the LEAP-RE program that received funding from the European Union's Horizon 2020 Research and Innovation Program under Grant Agreement 963530, the CNRS, the University of Lille and the Région Hauts-de-France. Dr. Ashwani Kumar greatly acknowledges CSIR-SRA (Pool Scientist), New Delhi for the funding (13(9131)A/2020-Pool) for the financial support to carry out this work.

#### References

- [1] O. Ellabban, H. Abu-Rub, F. Blaabjerg, Renewable energy resources: current status, future prospects and their enabling technology, *Renew. Sust. Energ. Rev.* 39 (2014) 748–764, <https://doi.org/10.1016/j.rser.2014.07.113>.
- [2] A.M. Omer, Energy, environment and sustainable development, *Renew. Sust. Energ. Rev.* 12 (2008) 2265–2300, <https://doi.org/10.1016/j.rser.2007.05.001>. [3] W. Ndambakuwa, Y. Ndambakuwa, J. Choi, G. Fernando, D. Neupane, S.R. Mishra, F. Perez, R.K. Gupta, Nanostructured nickel-cobalt oxide and sulfide for applications in supercapacitors and green energy production using waste water, *Surf. Coat. Technol.* 410 (2021) 126933, <https://doi.org/10.1016/j.surfcoat.2021.126933>.
- [4] S. Ould Amrouche, D. Rekioua, T. Rekioua, S. Bacha, Overview of energy storage in renewable energy systems, *Int. J. Hydrog. Energy* 41 (2016) 20914–20927, <https://doi.org/10.1016/j.ijhydene.2016.06.243>.
- [5] E. Pomerantseva, Y. Gogotsi, Two-dimensional heterostructures for energy storage, *Nat. Energy* 2 (2017) 1–6, <https://doi.org/10.1038/nenergy.2017.89>.
- [6] B. Anasori, M. Lukatskaya, Y. Gogotsi, 2D metal carbides and nitrides (MXenes) for energy storage, *Nat. Rev. Mater.* 2 (2017) 16098, <https://doi.org/10.1038/natrevmats.2016.98>.
- [7] F. Wang, S. Xiao, Y. Hou, C. Hu, L. Liu, Y. Wu, Electrode materials for aqueous asymmetric supercapacitors, *RSC Adv.* 3 (2013) 13059–13084, <https://doi.org/10.1039/c3ra23466e>.
- [8] R. Adalati, M. Sharma, A. Kumar, S. Sharma, R. Chandra, Metal nitride composite based nanostructured sheet-electrodes alternately stacked in asymmetric configuration towards robust flexible supercapacitor, *J. Energy Storage* 55 (2022) 105617, <https://doi.org/10.1016/j.est.2022.105617>.
- [9] S. Sharma, R. Adalati, M. Sharma, S. Jindal, A. Kumar, Single-step fabrication of dititanium nitride thin-film flexible and biocompatible supercapacitor, *Ceram. Int.* (2022), <https://doi.org/10.1016/j.ceramint.2022.08.055>.
- [10] Y. Wang, Y. Song, Y. Xia, Electrochemical capacitors: mechanism, materials, systems, characterization and applications, *Chem. Soc. Rev.* 45 (2016) 5925–5950, <https://doi.org/10.1039/c5cs00580a>.
- [11] A. Muzaffar, M.B. Ahamed, K. Deshmukh, J. Thirumalai, A review on recent advances in hybrid supercapacitors: design, fabrication and applications, *Renew. Sust. Energ. Rev.* 101 (2019) 123–145, <https://doi.org/10.1016/j.rser.2018.10.026>.
- [12] J. Libich, J. Máca, J. Vondrák, O. Čech, M. Sedlářková, Supercapacitors: properties and applications, *J. Energy Storage* 17 (2018) 224–227, <https://doi.org/10.1016/j.est.2018.03.012>.
- [13] Y. Gogotsi, R.M. Penner, Energy storage in nanomaterials - capacitive, pseudocapacitive, or battery-like? *ACS Nano* 12 (2018) 2081–2083, <https://doi.org/10.1021/acs.nano.8b01914>.
- [14] M. Sharma, R. Adalati, A. Kumar, V. Chawla, R. Chandra, Elevated performance of binder-free  $Co_3O_4$  electrode for the supercapacitor applications, *Nano Express* 2 (2021), <https://doi.org/10.1088/2632-959X/abd686>.
- [15] Q.Z. Zhang, D. Zhang, Z.C. Miao, X.L. Zhang, S.L. Chou, Research progress in  $MnO_2$ -carbon based supercapacitor electrode materials, *Small* 14 (2018) 1–15, <https://doi.org/10.1002/sml.201702883>.
- [16] M. Sharma, R. Adalati, A. Kumar, V. Chawla, R. Chandra, Single step fabrication of nanostructured  $Cr_2O_3$ - $MoO_2$  composite flexible electrode for top-notch asymmetric supercapacitor, *Appl. Surf. Sci.* 555 (2021) 149721, <https://doi.org/10.1016/j.apsusc.2021.149721>.
- [17] S. Venkateshalu, A.N. Grace,  $Ti_3C_2Tx$  MXene and vanadium nitride/Porous carbon as electrodes for asymmetric supercapacitors, *Electrochim. Acta* 341 (2020) 136035, <https://doi.org/10.1016/j.electacta.2020.136035>.
- [18] L.Q. Fan, G.J. Liu, J.H. Wu, L. Liu, J.M. Lin, Y.L. Wei, Asymmetric supercapacitor based on graphene oxide/polypyrrole composite and activated carbon electrodes, *Electrochim. Acta* 137 (2014) 26–33, <https://doi.org/10.1016/j.electacta.2014.05.137>.
- [19] M. Zhu, Q. Chen, J. Tang, W. Wei, S. Li, Core@shell  $\beta$ - $FeOOH$ @polypyrrole derived N, S-codoped  $Fe_3O_4$ @N-doped porous carbon nanococoons for high performance

- supercapacitors, *Appl. Surf. Sci.* 480 (2019) 582–592, <https://doi.org/10.1016/j.apsusc.2019.02.242>.
- [20] S. Chopra, A. Gupta, Y. Kumar, Recent studies on metal oxide and nitride based electrode material for supercapacitors application - a review, *compliance, Engineering Journal* 10 (2019) 18–36.
- [21] S. Ghosh, S.M. Jeong, S.R. Polaki, A review on metal nitrides/oxynitrides as an emerging supercapacitor electrode beyond oxide, *Korean J. Chem. Eng.* 35 (2018) 1389–1408, <https://doi.org/10.1007/s11814-018-0089-6>.
- [22] M.S. Balogun, W. Qiu, W. Wang, P. Fang, X. Lu, Y. Tong, Recent advances in metal nitrides as high-performance electrode materials for energy storage devices, *J. Mater. Chem. A* 3 (2015) 1364–1387, <https://doi.org/10.1039/c4ta05565a>.
- [23] M. Idrees, A. Mukhtar, S.M. Ata-ur-Rehman, Q. Abbas, X.Li Zhang, Transition metal nitride electrodes as future energy storage devices: a review, *Mater. Today Commun.* 27 (2021) 102363, <https://doi.org/10.1016/j.mtcomm.2021.102363>.
- [24] T. Liu, Y. Li, Addressing the Achilles' heel of pseudocapacitive materials: longterm stability, *InfoMat.* 2 (2020) 807–842, <https://doi.org/10.1002/inf2.12105>.
- [25] S. Mahadik, S. Surendran, J.Y. Kim, G. Janani, D.-K. Lee, T.-H. Kim, J.K. Kim, U. Sim, Syntheses and electronic structure engineering of transition metal nitrides for supercapacitor applications, *J. Mater. Chem. A* (2022), <https://doi.org/10.1039/d2ta02584a>.
- [26] F. Bu, W. Zhou, Y. Xu, Y. Du, C. Guan, W. Huang, Recent developments of advanced micro-supercapacitors: design, fabrication and applications, *Npj Flex. Electron.* 4 (2020), <https://doi.org/10.1038/s41528-020-00093-6>.
- [27] C. Zhu, P. Yang, D. Chao, X. Wang, X. Zhang, S. Chen, B.K. Tay, H. Huang, H. Zhang, W. Mai, H.J. Fan, All metal nitrides solid-state asymmetric supercapacitors, *Adv. Mater.* 27 (2015) 4566–4571, <https://doi.org/10.1002/adma.201501838>.
- [28] M. Sevilla, A.B. Fuertes, Direct synthesis of highly porous interconnected carbon nanosheets and their application as high-performance supercapacitors, *ACS Nano* 8 (2014) 5069–5078, <https://doi.org/10.1021/nn501124h>.
- [29] S. Jin, H. Lee, S. Yim, Enhanced capacitive properties of all-metal-oxidenanoparticle-based asymmetric supercapacitors, *RSC Adv.* 9 (2019) 31846–31852, <https://doi.org/10.1039/c9ra06066a>.
- [30] M. Sharma, R. Adalati, A. Kumar, M. Mehta, R. Chandra, Composite assembling of oxide-based optically transparent electrodes for high-performance asymmetric supercapacitors, *ACS Appl. Mater. Interfaces* (2022), <https://doi.org/10.1021/acsami.2c05189>.
- [31] Y. Xiao, Y. Xu, K. Zhang, X. Tang, J. Huang, K. Yuan, Y. Chen, Coaxial electrospun free-standing and mechanical stable hierarchical porous carbon nanofiber membrane for flexible supercapacitors, *Carbon* 160 (2020) 80–87, <https://doi.org/10.1016/j.carbon.2020.01.017>.
- [32] Y. Xiao, J. Huang, Y. Xu, K. Yuan, Y. Chen, Facile and scalable fabrication of nitrogen-doped porous carbon nanosheets for capacitive energy storage with ultrahigh energy density, *ACS Appl. Mater. Interfaces* 11 (2019) 20029–20036, <https://doi.org/10.1021/acsami.9b04393>.
- [33] R. Jamil, D.S. Silvester, Ionic liquid gel polymer electrolytes for flexible supercapacitors: challenges and prospects, *Curr. Opin. Electrochem.* 35 (2022) 101046, <https://doi.org/10.1016/j.coelec.2022.101046>.
- [34] R. Zhang, A. Ahmed, B. Yu, H. Cong, Y. Shen, Preparation, application and development of poly(ionic liquid) microspheres, *J. Mol. Liq.* 362 (2022) 119706, <https://doi.org/10.1016/j.molliq.2022.119706>.
- [35] H. Liang, C. Xia, A.H. Emwas, D.H. Anjum, X. Miao, H.N. Alshareef, Phosphine plasma activation of  $\alpha$ -Fe<sub>2</sub>O<sub>3</sub> for high energy asymmetric supercapacitors, *Nano Energy* 49 (2018) 155–162, <https://doi.org/10.1016/j.nanoen.2018.04.032>.
- [36] J. Liu, L. Zhang, H. Bin Wu, J. Lin, Z. Shen, X.W. Lou, High-performance flexible asymmetric supercapacitors based on a new graphene foam/carbon nanotube hybrid film, *Energy Environ. Sci.* 7 (2014) 3709–3719, <https://doi.org/10.1039/c4ee01475h>.
- [37] J. Hao, L. Yuan, C. Ye, D. Chao, K. Davey, Z. Guo, S.Z. Qiao, Boosting zinc electrode reversibility in aqueous electrolytes by using low-cost antisolvents, *Angew. Chem. Int. Ed.* 60 (2021) 7366–7375, <https://doi.org/10.1002/anie.202016531>.
- [38] J. Huang, K. Yuan, Y. Chen, Wide voltage aqueous asymmetric supercapacitors: advances, strategies, and challenges, *Adv. Funct. Mater.* 32 (2022), <https://doi.org/10.1002/adfm.202108107>.
- [39] Y. Cao, J. Liang, X. Li, L. Yue, Q. Liu, S. Lu, A.M. Asiri, J. Hu, Y. Luo, X. Sun, Recent advances in perovskite oxides as electrode materials for supercapacitors, *Chem. Commun.* 57 (2021) 2343–2355, <https://doi.org/10.1039/d0cc07970g>.
- [40] Y. Zhang, Q. Zhong, Y. Bu, D. Meng, H. Gu, Q. Lu, Y. Zhao, G. Zhu, Advances and perspectives for the application of perovskite oxides in supercapacitors, *Energy Fuels* 35 (2021) 17353–17371, <https://doi.org/10.1021/acs.energyfuels.1c03157>.
- [41] A.B. Dongil, Recent progress on transition metal nitrides nanoparticles as heterogeneous catalysts, *Nanomaterials* 9 (2019) 1111, <https://doi.org/10.3390/nano9081111>.
- [42] D.P. Chatterjee, A.K. Nandi, A review on the recent advances in hybrid supercapacitors, *J. Mater. Chem. A* 9 (2021) 15880–15918, <https://doi.org/10.1039/d1ta02505h>.
- [43] M. Tomy, A.Ambika Rajappan, V. VM, X.Thankappan Suryabai, Emergence of novel 2D materials for high-performance supercapacitor electrode applications: a brief review, *Energy and Fuels* 35 (2021) 19881–19900, <https://doi.org/10.1021/acs.energyfuels.1c02743>.
- [44] M. Sajjad, M. Amin, M.S. Javed, M. Imran, W. Hu, Z. Mao, W. Lu, Recent trends in transition metal diselenides (XSe<sub>2</sub>: X = ni, mn, Co) and their composites for high energy faradic supercapacitors, *J. Energy Storage* 43 (2021) 103176, <https://doi.org/10.1016/j.est.2021.103176>.
- [45] A. Kumar, R. Adalati, M. Kaushik, Y. Kumar, R. Chandra, Catalyst free MnO<sub>2</sub> nanoflakes for electrochemical capacitor, *J. Electrochem. Soc.* 167 (11) (2020) 116509, <https://doi.org/10.1149/1945-7111/aba369>.
- [46] R. Adalati, A. Kumar, G. Malik, R. Chandra, Transition metal nitride nanoflake thin film grown by DC-magnetron sputtering for high-performance supercapacitor applications, *AIP Conf. Proc.* 2265 (2020) 0–3, <https://doi.org/10.1063/5.0016764>.
- [47] X. Lu, G. Wang, T. Zhai, M. Yu, S. Xie, Y. Ling, C. Liang, Y. Tong, Y. Li, Stabilized TiN nanowire arrays for high-performance and flexible supercapacitors, *Nano Lett.* 12 (2012) 5376–5381, <https://doi.org/10.1021/nl302761z>.
- [48] S. Liu, K.V. Sankar, A. Kundu, M. Ma, J.Y. Kwon, S.C. Jun, Honeycomb-like interconnected network of nickel phosphide heteronanoparticles with superior electrochemical performance for supercapacitors, *ACS Appl. Mater. Interfaces* 9 (2017) 21829–21838, <https://doi.org/10.1021/acsami.7b05384>.
- [49] M. Yeager, W. Du, R. Si, D. Su, N. Mariniković, X. Teng, Highly efficient K<sub>0.15</sub>MnO<sub>2</sub> birnessite nanosheets for stable pseudocapacitive cathodes, *J. Phys. Chem. C* 116 (2012) 20173–20181, <https://doi.org/10.1021/jp304809r>.
- [50] J. Zhao, S. Xu, K. Tschulik, R.G. Compton, M. Wei, D. O'Hare, D.G. Evans, X. Duan, Molecular-scale hybridization of clay monolayers and conducting polymer for thin-film supercapacitors, *Adv. Funct. Mater.* 25 (2015) 2745–2753, <https://doi.org/10.1002/adfm.201500408>.
- [51] N. Base, Materials science of carbides, nitrides and borides, *Mater. Sci. Carbides, Nitrides Borides* (1999), <https://doi.org/10.1007/978-94-011-4562-6>.
- [52] M. Acerce, D. Voiry, M. Chhowalla, Metallic 1T phase MoS<sub>2</sub> nanosheets as supercapacitor electrode materials, *Nat. Nanotechnol.* 10 (2015) 313–318, <https://doi.org/10.1038/nnano.2015.40>.
- [53] Z. Jacob, I.I. Smolyaninov, E.E. Narimanov, Broadband Purcell effect: radiative decay engineering with metamaterials, *Appl. Phys. Lett.* 100 (2012) 534–537, <https://doi.org/10.1063/1.4710548>.
- [54] S.G. Brush, Comments on "on the distortion of the history of science in science education", *Sci. Educ.* 63 (1979) 277–278, <https://doi.org/10.1002/sce.3730630217>.
- [55] J.K. Nørskov, F. Abild-Pedersen, F. Studt, T. Bligaard, Density functional theory in surface chemistry and catalysis, *Proc. Natl. Acad. Sci. U. S. A.* 108 (2011) 937–943, <https://doi.org/10.1073/pnas.1006652108>.
- [56] A. Costales, M.A. Blanco, Á. Martín Pendás, A.K. Kandalam, R. Pandey, Chemical bonding in group III nitrides, *J. Am. Chem. Soc.* 124 (2002) 4116–4123, <https://doi.org/10.1021/ja017380o>.
- [57] S.A. Jansen, R. Hoffmann, Surface chemistry of transition metal carbides: a theoretical analysis, *Surf. Sci.* 197 (1988) 474–508, [https://doi.org/10.1016/0039-6028\(88\)90641-3](https://doi.org/10.1016/0039-6028(88)90641-3).
- [58] C. Giordano, M. Antonietti, Synthesis of crystalline metal nitride and metal carbide nanostructures by sol-gel chemistry, *Nano Today* 6 (2011) 366–380, <https://doi.org/10.1016/j.nantod.2011.06.002>.
- [59] W.F. Chen, J.T. Muckerman, E. Fujita, Recent developments in transition metal carbides and nitrides as hydrogen evolution electrocatalysts, *Chem. Commun.* 49 (2013) 8896–8909, <https://doi.org/10.1039/c3cc44076a>.
- [60] A.M. Alexander, J.S.J. Hargreaves, Alternative catalytic materials: carbides, nitrides, phosphides and amorphous boron alloys, *Chem. Soc. Rev.* 39 (2010) 4388–4401, <https://doi.org/10.1039/b916787k>.
- [61] U.v. Alpen, A. Rabenau, G.H. Talat, Ionic conductivity in Li<sub>3</sub>N single crystals, *Appl. Phys. Lett.* 30 (1977) 621–623, <https://doi.org/10.1063/1.89283>.
- [62] I. Ashraf, S. Rizwan, M. Iqbal, A comprehensive review on the synthesis and energy applications of Nano-structured metal nitrides, *Front. Mater.* 7 (2020) 1–20, <https://doi.org/10.3389/fmats.2020.00181>.
- [63] S.V. Didziulis, K.D. Butcher, S.S. Perry, Small cluster models of the surface electronic structure and bonding properties of titanium carbide, vanadium carbide, and titanium nitride, *Inorg. Chem.* 42 (2003) 7766–7781, <https://doi.org/10.1021/ic030140k>.
- [64] H.W. Hugosson, O. Eriksson, U. Jansson, A.V. Ruban, P. Souvatzis, I.A. Abrikosov, Surface energies and work functions of the transition metal carbides, *Surf. Sci.* 557 (2004) 243–254, <https://doi.org/10.1016/j.susc.2004.03.050>.
- [65] Y. Zhou, W. Guo, T. Li, A review on transition metal nitrides as electrode materials for supercapacitors, *Ceram. Int.* 45 (2019) 21062–21076, <https://doi.org/10.1016/j.ceramint.2019.07.151>.
- [66] S.H. Gage, B.G. Trewyn, C.V. Ciobanu, S. Pylypenko, R.M. Richards, Synthetic advancements and catalytic applications of nickel nitride, *catal. Sci. Technol.* 6 (2016) 4059–4076, <https://doi.org/10.1039/c6cy00712k>.
- [67] M.S. Balogun, M. Yu, C. Li, T. Zhai, Y. Liu, X. Lu, Y. Tong, Facile synthesis of titanium nitride nanowires on carbon fabric for flexible and high-rate lithium ion batteries, *J. Mater. Chem. A* 2 (2014) 10825–10829, <https://doi.org/10.1039/c4ta00987h>.
- [68] E.G. Gillan, R.B. Kaner, Synthesis of refractory ceramics via rapid metathesis reactions between solid-state precursors, *Chem. Mater.* 8 (1996) 333–343, <https://doi.org/10.1021/cm950232a>.
- [69] G. Malik, S. Mourya, R. Adalati, R. Chandra, Nanostructured RF sputtered hexagonal ZnO nano-pebbles based electrode material for energy efficient devices, *AIP Conf. Proc.* 2265 (2020), <https://doi.org/10.1063/5.0016750>.
- [70] A. Kumar, G. Malik, R. Adalati, V. Chawla, M.K. Pandey, R. Chandra, Tuning the wettability of highly transparent Nb<sub>2</sub>O<sub>5</sub> nano-sliced coatings to enhance anticorrosion property, *Mater. Sci. Semicond. Process.* 123 (2021) 105513, <https://doi.org/10.1016/j.mssp.2020.105513>.
- [71] M.Z. Xue, Z.W. Fu, Electrochemical reactions of lithium with transition metal stannides, *Solid State Ionics* 177 (2006) 1501–1507, <https://doi.org/10.1016/j.ssi.2006.07.030>.



- [72] S. Ramanathan, S.T. Oyama, New catalysts for hydroprocessing: transition metal carbides and nitrides, *J. Phys. Chem.* 99 (1995) 16365–16372, <https://doi.org/10.1021/j100044a025>.
- [73] K. Leinenweber, M. O’Keeffe, M. Somayazulu, H. Hubert, P.F. McMillan, G.H. Wolf, Synthesis and structure refinement of the spinel,  $\gamma$ -Ge<sub>3</sub>N<sub>4</sub>, *Chem. A Eur. J.* 5 (1999) 3076–3078, [https://doi.org/10.1002/\(SICI\)1521-3765\(19991001\)5](https://doi.org/10.1002/(SICI)1521-3765(19991001)5).
- [74] G. Serghiou, G. Miehle, O. Tschauner, A. Zerr, R. Boehler, Synthesis of a cubic Ge<sub>3</sub>N<sub>4</sub> phase at high pressures and temperatures, *J. Chem. Phys.* 111 (1999) 4659–4662, <https://doi.org/10.1063/1.479227>.
- [75] B. Mazumder, A.L. Hector, Synthesis and applications of nanocrystalline nitride materials, *J. Mater. Chem.* 19 (2009) 4673–4686, <https://doi.org/10.1039/b817407e>.
- [76] Y. Zhong, X.H. Xia, F. Shi, J.Y. Zhan, J.P. Tu, H.J. Fan, Transition metal carbides and nitrides in energy storage and conversion, *Adv. Sci.* 3 (2015) 1500286, <https://doi.org/10.1002/advs.201500286>.
- [77] X. Tian, J. Luo, H. Nan, H. Zou, R. Chen, T. Shu, X. Li, Y. Li, H. Song, S. Liao, R.R. Adzic, Transition metal nitride coated with atomic layers of Pt as a low-cost, highly stable electrocatalyst for the oxygen reduction reaction, *J. Am. Chem. Soc.* 138 (2016) 1575–1583, <https://doi.org/10.1021/jacs.5b11364>.
- [78] E.G. Gillan, R.B. Kaner, Rapid solid-state synthesis of refractory nitrides, *Inorg. Chem.* 33 (1994) 5693–5700, <https://doi.org/10.1021/ic00103a015>.
- [79] W. Bi, Z. Hu, X. Li, C. Wu, J. Wu, Y. Wu, Y. Xie, Metallic mesocrystal nanosheets of vanadium nitride for high-performance all-solid-state pseudocapacitors, *Nano Res.* 8 (2015) 193–200, <https://doi.org/10.1007/s12274-014-0612-y>.
- [80] H. Wang, J. Li, K. Li, Y. Lin, J. Chen, L. Gao, V. Nicolosi, X. Xiao, J.M. Lee, Transition metal nitrides for electrochemical energy applications, *Chem. Soc. Rev.* 50 (2021) 1354–1390, <https://doi.org/10.1039/d0cs00415d>.
- [81] Biao Gao, Xingxing Li, Kang Ding, Chao Huang, Qingwei Li, Paul K. Chu, Kaifu Huo, Recent progress in nanostructured transition metal nitrides for advanced electrochemical energy storage, *J. Mater. Chem. A* 7 (1) (2019) 14–37, <https://doi.org/10.1039/c8ta05760e>.
- [82] S. Dong, X. Chen, X. Zhang, G. Cui, Nanostructured transition metal nitrides for energy storage and fuel cells, *Coord. Chem. Rev.* 257 (2013) 1946–1956, <https://doi.org/10.1016/j.ccr.2012.12.012>.
- [83] F.J. Owens, Electronic properties, *Phys. Low Dimens. Mater.* 31 (2017) 15–28, [https://doi.org/10.1142/9789813225862\\_0002](https://doi.org/10.1142/9789813225862_0002).
- [84] Jean-Louis Calais, Band structure of transition metal compounds, *Adv. Phys.* 26 (6) (1977) 847–885, <https://doi.org/10.1080/00018737700101473>.
- [85] J. Xie, Y. Xie, Transition metal nitrides for electrocatalytic energy conversion: opportunities and challenges, *Chem. A Eur. J.* 22 (2016) 3588–3598, <https://doi.org/10.1002/chem.201501120>.
- [86] B. Gao, X. Li, K. Ding, C. Huang, Q. Li, P.K. Chu, K. Huo, Recent progress in nanostructured transition metal nitrides for advanced electrochemical energy storage, *J. Mater. Chem. A* 7 (2019) 14–37, <https://doi.org/10.1039/c8ta05760e>.
- [87] S.I.U. Shah, A.L. Hector, J.R. Owen, Redox supercapacitor performance of nanocrystalline molybdenum nitrides obtained by ammonolysis of chloride- and amide-derived precursors, *J. Power Sources* 266 (2014) 456–463, <https://doi.org/10.1016/j.jpowsour.2014.05.045>.
- [88] A. Achour, R.L. Porto, M.A. Soussou, M. Islam, M. Boujtita, K.A. Aissa, L. Le Brizoul, A. Djouadi, T. Brousse, Titanium nitride films for micro-supercapacitors: effect of surface chemistry and film morphology on the capacitance, *J. Power Sources* 300 (2015) 525–532, <https://doi.org/10.1016/j.jpowsour.2015.09.012>.
- [89] E. Eustache, R. Frappier, R.L. Porto, S. Bouhtiyaa, J.F. Pierson, T. Brousse, Asymmetric electrochemical capacitor microdevice designed with vanadium nitride and nickel oxide thin film electrodes, *Electrochem. Commun.* 28 (2013) 104–106, <https://doi.org/10.1016/j.elecom.2012.12.015>.
- [90] Daiwon Choi, Prashant N. Kumta, Chemically synthesized nanostructured VN for pseudocapacitor application, *Electrochim. Solid-State Lett.* 8 (8) (2005) A418, <https://doi.org/10.1149/1.1951201>.
- [91] M.S. Balogun, Y. Zeng, W. Qiu, Y. Luo, A. Onasanya, T.K. Olaniyi, Y. Tong, Three-dimensional nickel nitride (Ni<sub>3</sub>N) nanosheets: free standing and flexible electrodes for lithium ion batteries and supercapacitors, *J. Mater. Chem. A* 4 (2016) 9844–9849, <https://doi.org/10.1039/c6ta02492k>.
- [92] B. Wei, C. Shang, L. Shui, X. Wang, G. Zhou, TiVN composite hollow mesospheres for high-performance supercapacitors, *Materials Research Express* 6 (2) (2018) 025801, <https://doi.org/10.1088/2053-1591/aaed08>.
- [93] V. Sridhar, H. Park, Manganese nitride stabilized on reduced graphene oxide substrate for high performance sodium ion batteries, super-capacitors and EMI shielding, *J. Alloys Compd.* 808 (2019) 151748, <https://doi.org/10.1016/j.jallcom.2019.151748>.
- [94] H. Cui, G. Zhu, X. Liu, F. Liu, Y. Xie, C. Yang, T. Lin, H. Gu, F. Huang, Niobium nitride Nb<sub>4</sub>N<sub>5</sub> as a new high-performance electrode material for supercapacitors, *Adv. Sci.* 2 (2015) 1–12, <https://doi.org/10.1002/advs.201500126>.
- [95] J. Liu, C. Hu, W. Gao, H. Li, Y. Zhao, Combined enhanced redox kinetics and physicochemical confinement in three-dimensionally ordered macro/mesoporous TiN for highly stable lithium-sulfur batteries, *Nanotechnology* 33 (2022), <https://doi.org/10.1088/1361-6528/ac3e30>.
- [96] Y. Yuan, J. Wang, S. Adimi, H. Shen, T. Thomas, R. Ma, J.P. Attfield, M. Yang, Zirconium nitride catalysts surpass platinum for oxygen reduction, *Nat. Mater.* 19 (2020) 282–286, <https://doi.org/10.1038/s41563-019-0535-9>.
- [97] X. Yang, J. Nash, J. Anibal, M. Dunwell, S. Kattel, E. Stavitski, K. Attenkofer, J.G. Chen, Y. Yan, B. Xu, Mechanistic insights into electrochemical nitrogen reduction reaction on vanadium nitride nanoparticles, *J. Am. Chem. Soc.* 140 (2018) 13387–13391, <https://doi.org/10.1021/jacs.8b08379>.
- [98] J. Lee, S. Kim, J.H. Park, C. Jo, J. Chun, Y.E. Sung, E. Lim, J. Lee, A small-strain niobium nitride anode with ordered mesopores for ultra-stable potassium-ion batteries, *J. Mater. Chem. A* 8 (2020) 3119–3127, <https://doi.org/10.1039/c9ta11663j>.
- [99] F. Zhang, S. Xi, G. Lin, X. Hu, X.W. (David) Lou, K. Xie, Metallic porous iron nitride and tantalum nitride single crystals with enhanced electrocatalysis performance, *Adv. Mater.* 31 (2019) 1–7, <https://doi.org/10.1002/adma.201806552>.
- [100] B. Wei, G. Mei, H. Liang, Z. Qi, D. Zhang, H. Shen, Z. Wang, Porous CrN thin films by selectively etching CrCuN for symmetric supercapacitors, *J. Power Sources* 385 (2018) 39–44, <https://doi.org/10.1016/j.jpowsour.2018.03.023>.
- [101] H. Jin, X. Liu, A. Vasileff, Y. Jiao, Y. Zhao, Y. Zheng, S.Z. Qiao, Single-crystal nitrogen-rich two-dimensional Mo<sub>5</sub>N<sub>6</sub> nanosheets for efficient and stable seawater splitting, *ACS Nano* 12 (2018) 12761–12769, <https://doi.org/10.1021/acsnano.8b07841>.
- [102] H. Yu, X. Yang, X. Xiao, M. Chen, Q. Zhang, L. Huang, J. Wu, T. Li, S. Chen, L. Song, L. Gu, B. Y. Xia, G. Feng, J. Li, J. Zhou, Atmospheric-pressure synthesis of 2D nitrogen-rich tungsten nitride, *Adv. Mater.* 30 (2018) 1–7, <https://doi.org/10.1002/adma.201805655>.
- [103] C. Walter, P.W. Menezes, S. Orthmann, J. Schuch, P. Connor, B. Kaiser, M. Lerch, M. Driess, A molecular approach to manganese nitride acting as a high performance electrocatalyst in the oxygen evolution reaction, *Angew. Chem. Int. Ed.* 130 (2018) 706–710, <https://doi.org/10.1002/ange.201710460>.
- [104] D. Liu, X. Xu, J. Tan, J. Zhu, Q. Li, Y. Luo, P. Wu, X. Zhang, C. Han, L. Mai, Micrometer-sized porous Fe<sub>2</sub>N/C bulk for high-areal-capacity and stable lithium storage, *Small* 15 (2019) 1–9, <https://doi.org/10.1002/sml.201803572>.
- [105] Z. Chen, Y. Song, J. Cai, X. Zheng, D. Han, Y. Wu, Y. Zang, S. Niu, Y. Liu, J. Zhu, X. Liu, G. Wang, Tailoring the d-band centers enables Co<sub>4</sub>N nanosheets to be highly active for hydrogen evolution catalysis, *Angew. Chem. Int. Ed.* 130 (2018) 5170–5174, <https://doi.org/10.1002/ange.201801834>.
- [106] B. Liu, B. He, H.Q. Peng, Y. Zhao, J. Cheng, J. Xia, J. Shen, T.W. Ng, X. Meng, C.S. Lee, W. Zhang, Unconventional nickel nitride enriched with nitrogen vacancies as a high-efficiency electrocatalyst for hydrogen evolution, *Adv. Sci.* 5 (2018) 1–7, <https://doi.org/10.1002/advs.201800406>.
- [107] Z.Q. Liang, T.T. Zhuang, A. Seifitokaldani, J. Li, C.W. Huang, C.S. Tan, Y. Li, P. De Luna, C.T. Dinh, Y. Hu, Q. Xiao, P.L. Hsieh, Y. Wang, F. Li, R. Quintero-Bermudez, Y. Zhou, P. Chen, Y. Pang, S.C. Lo, L.J. Chen, H. Tan, Z. Xu, S. Zhao, D. Sinton, E.H. Sargent, Copper-nitride enhances the stable electrosynthesis of multi-carbon products from CO<sub>2</sub>, *Nat. Commun.* 9 (2018) 1–8, <https://doi.org/10.1038/s41467-018-06311-0>.
- [108] X. Lu, M. Yu, T. Zhai, G. Wang, S. Xie, T. Liu, C. Liang, Y. Tong, Y. Li, Erratum: high energy density asymmetric quasi-solid-state supercapacitor based on porous vanadium nitride nanowire anode, *Nano Lett.* 20 (2020) 6932, <https://doi.org/10.1021/acs.nanolett.0c03076>.
- [109] X. Lu, M. Yu, T. Zhai, G. Wang, S. Xie, T. Liu, C. Liang, Y. Tong, Y. Li, High energy density asymmetric quasi-solid-state supercapacitor based on porous vanadium nitride nanowire anode, *Nano Lett.* 13 (2013) 2628–2633, <https://doi.org/10.1021/nl400760a>.
- [110] M. Chen, H. Fan, Y. Zhang, X. Liang, Q. Chen, X. Xia, Coupling PEDOT on mesoporous vanadium nitride arrays for advanced flexible all-solid-state supercapacitors, *Small* 16 (2020) 1–9, <https://doi.org/10.1002/sml.202003434>. [111] R. Lucio-Porto, S. Bouhtiyaa, J.F. Pierson, A. Morel, F. Capon, P. Boulet, T. Brousse, VN thin films as electrode materials for electrochemical capacitors, *Electrochim. Acta* 141 (2014) 203–211, <https://doi.org/10.1016/j.electacta.2014.07.056>.
- [112] Y. Wu, Y. Yang, X. Zhao, Y. Tan, Y. Liu, Z. Wang, F. Ran, A novel hierarchical porous 3D structured vanadium Nitride/Carbon membranes for high-performance supercapacitor negative electrodes, *Nano-Micro Lett.* 10 (2018) 1–11, <https://doi.org/10.1007/s40820-018-0217-1>.
- [113] G. Durai, P. Kuppusami, T. Maiyalagan, J. Theerthagiri, P. Vinoth Kumar, H.S. Kim, Influence of chromium content on microstructural and electrochemical supercapacitive properties of vanadium nitride thin films developed by reactive magnetron co-sputtering process, *Ceram. Int.* 45 (2019) 12643–12653, <https://doi.org/10.1016/j.ceramint.2019.02.170>.
- [114] R. Adalati, A. Kumar, Y. Kumar, R. Chandra, A high-performing asymmetric supercapacitor of molybdenum nitride and vanadium nitride thin films as binderfree electrode grown through reactive sputtering, *Energy Technol.* (2020), <https://doi.org/10.1002/ente.202000466>.
- [115] R. Adalati, A. Kumar, M. Sharma, R. Chandra, Pt enhanced capacitive performance of Cr<sub>2</sub>N electrode toward flexible asymmetric supercapacitor, *Appl. Phys. Lett.* 118 (2021), <https://doi.org/10.1063/5.0047038>.
- [116] M. Zhang, Z. Xiong, J. Jia, Z. Zhou, B. Wu, Y. Ni, X. Zhou, L. Cao, Improving electrochemical performance of hollow Cr<sub>2</sub>O<sub>3</sub>/CrN nanoshells as electrode materials for supercapacitors, *J. Electroanal. Chem.* 856 (2020) 113696, <https://doi.org/10.1016/j.jelechem.2019.113696>.
- [117] Z. Qi, B. Wei, J. Wang, Y. Yang, Z. Wang, Nanostructured porous CrN thin films by oblique angle magnetron sputtering for symmetric supercapacitors, *J. Alloys Compd.* 806 (2019) 953–959, <https://doi.org/10.1016/j.jallcom.2019.07.325>.
- [118] X. Xu, S. Chang, Z. Hong, Y. Zeng, H. Zhang, P. Li, S. Zheng, Z. Wang, S. Duo, Construction of 3D CrN@nitrogen-doped carbon nanosheet arrays by reactive magnetron sputtering for the free-standing electrode of supercapacitor, *Nanotechnology* 33 (2022) 055402, <https://doi.org/10.1088/1361-6528/ac3356>.
- [119] P. Chen, K. Xu, Y. Tong, X. Li, S. Tao, Z. Fang, W. Chu, X. Wu, C. Wu, Cobalt nitrides as a class of metallic electrocatalysts for the oxygen evolution reaction, *Inorg. Chem. Front.* 3 (2016) 236–242, <https://doi.org/10.1039/c5qu00197h>.

- [120] H. Zhang, W. Hu, B. Wei, J. Zheng, Z. Qi, Z. Wang, Freestanding Co<sub>3</sub>N thin film for high performance supercapacitors, *Ceram. Int.* 47 (2021) 3267–3271, <https://doi.org/10.1016/j.ceramint.2020.09.166>.
- [121] X. Liu, W. Zang, C. Guan, L. Zhang, Y. Qian, A.M. Elshahawy, D. Zhao, S.J. Pennycook, J. Wang, Ni-doped cobalt-cobalt nitride heterostructure arrays for high-power supercapacitors, *ACS Energy Lett.* 3 (2018) 2462–2469, <https://doi.org/10.1021/acscenergylett.8b01393>.
- [122] R. Adalati, A. Kumar, M. Sharma, P. Tiwari, R. Chandra, Catalyst free approach for the fabrication of CoN//Zn<sub>3</sub>N<sub>2</sub> asymmetric configuration for highly efficient flexible supercapacitor, *Appl. Phys. Lett.* 117 (2020), <https://doi.org/10.1063/5.0019483>.
- [123] D.K. Nandi, U.K. Sen, S. Sinha, A. Dhara, S. Mitra, S.K. Sarkar, Atomic layer deposited tungsten nitride thin films as a new lithium-ion battery anode, *Phys. Chem. Chem. Phys.* 17 (2015) 17445–17453, <https://doi.org/10.1039/c5cp02184g>.
- [124] A. Ponrouch, Damien Monti, Andrea Boschini, Bengt Steen, Patrik Johansson, M. Rosa Palacin, Non-aqueous electrolytes for sodium-ion batteries, *J. Mater. Chem. A* 3 (1) (2015) 22–42, <https://doi.org/10.1039/C4TA04428B>.
- [125] S. Ouendi, K. Robert, D. Stievenard, T. Brousse, P. Roussel, C. Lethien, Sputtered tungsten nitride films as pseudocapacitive electrode for on chip microsupercapacitors, *Energy Storage Mater.* 20 (2019) 243–252, <https://doi.org/10.1016/j.ensm.2019.04.006>.
- [126] R. Prakash, A. Kumar, A. Pandey, D. Kaur, Binder free and high performance of sputtered tungsten nitride thin film electrode for supercapacitor device, *Int. J. Hydrog. Energy* 44 (2019) 10823–10832, <https://doi.org/10.1016/j.ijhydene.2019.02.005>.
- [127] A. Salman, S. Padmajan Sasikala, I.H. Kim, J.T. Kim, G.S. Lee, J.G. Kim, S.O. Kim, Tungsten nitride-coated graphene fibers for high-performance wearable supercapacitors, *Nanoscale* 12 (2020) 20239–20249, <https://doi.org/10.1039/d0nr06636b>.
- [128] R. Yu, X. Chong, Y. Jiang, R. Zhou, W. Yuan, J. Feng, The stability, electronic structure, elastic and metallic properties of manganese nitrides, *RSC Adv.* 5 (2015) 1620–1627, <https://doi.org/10.1039/c4ra10914g>.
- [129] G. Durai, P. Kuppusami, T. Maiyalagan, M. Ahila, P. Vinoth Kumar, Supercapacitive properties of manganese nitride thin film electrodes prepared by reactive magnetron sputtering: effect of different electrolytes, *Ceram. Int.* 45 (2019) 17120–17127, <https://doi.org/10.1016/j.ceramint.2019.05.265>.
- [130] W.-B. Zhang, X.-J. Ma, L.-B. Kong, Y.-C. Luo, L. Kang, Capacitive intermetallic manganese nitride with high volumetric energy densities, *J. Electrochem. Soc.* 163 (2016) A2830–A2834, <https://doi.org/10.1149/2.0141614jes>.
- [131] Y.-J. (Bernie) Ting, K. Lian, N. Kherani, in: Fabrication of Titanium Nitride and Molybdenum Nitride for Supercapacitor Electrode Application, ECS Meet. Abstr. MA2011-01, 2011, p. 265, <https://doi.org/10.1149/ma2011-01/6/265>.
- [132] N. Sun, D. Zhou, W. Liu, S. Shi, Z. Tian, F. Liu, S. Li, J. Wang, F. Ali, Tailoring surface chemistry and morphology of titanium nitride electrode for on-chip supercapacitors, *ACS Sustain. Chem. Eng.* 8 (2020) 7869–7878, <https://doi.org/10.1021/acssuschemeng.0c00977>.
- [133] A. Achour, R. Lucio-Porto, M. Chaker, A. Arman, A. Ahmadipourian, M.A. Soussou, M. Boujtitia, L. Le Brizoual, M.A. Djouadi, T. Brousse, Titanium vanadium nitride electrode for micro-supercapacitors, *Electrochem. Commun.* 77 (2017) 40–43, <https://doi.org/10.1016/j.elecom.2017.02.011>.
- [134] E. Kao, C. Yang, R. Warren, A. Kozinda, L. Lin, ALD titanium nitride coated carbon nanotube electrodes for electrochemical supercapacitors, in: 2015 Transducers - 2015 18th Int. Conf. Solid-State Sensors, Actuators Microsystems, TRANSDUCERS 2015, 2015, pp. 498–501, <https://doi.org/10.1109/TRANSDUCERS.2015.7180969>.
- [135] S.A. Ansari, N.A. Khan, Z. Hasan, A.A. Shaikh, F.K. Ferdousi, H.R. Barai, N.S. Lopa, M.M. Rahman, Electrochemical synthesis of titanium nitride nanoparticles onto titanium foil for electrochemical supercapacitors with ultrafast charge/discharge, *Sustain. Energy Fuel* 4 (2020) 2480–2490, <https://doi.org/10.1039/d0se00049c>.
- [136] M.B. Kanoun, S. Goumri-Said, M. Jaouen, Structure and mechanical stability of molybdenum nitrides: a first-principles study, *Phys. Rev. B Condens. Matter Mater. Phys.* 76 (2007) 2–5, <https://doi.org/10.1103/PhysRevB.76.134109>.
- [137] A.Y. Ganin, L. Kienle, G.V. Vajenine, Synthesis and characterisation of hexagonal molybdenum nitrides, *J. Solid State Chem.* 179 (2006) 2339–2348, <https://doi.org/10.1016/j.jssc.2006.05.025>.
- [138] C.L. Bull, P.F. McMillan, E. Soignard, K. Leinenweber, Determination of the crystal structure of δ-MoN by neutron diffraction, *J. Solid State Chem.* 177 (2004) 1488–1492, <https://doi.org/10.1016/j.jssc.2003.11.033>.
- [139] A.G. Cairns, J.G. Gallagher, J.S.J. Hargreaves, D. McKay, E. Morrison, J.L. Rico, K. Wilson, The influence of precursor source and thermal parameters upon the formation of beta-phase molybdenum nitride, *J. Alloys Compd.* 479 (2009) 851–854, <https://doi.org/10.1016/j.jallcom.2009.01.065>.
- [140] D. McKay, J.S.J. Hargreaves, J.L. Rico, J.L. Rivera, X.L. Sun, The influence of phase and morphology of molybdenum nitrides on ammonia synthesis activity and reduction characteristics, *J. Solid State Chem.* 181 (2008) 325–333, <https://doi.org/10.1016/j.jssc.2007.12.001>.
- [141] M.K. Neylon, S. Choi, H. Kwon, K.E. Curry, L.T. Thompson, Catalytic properties of early transition metal nitrides and carbides: n-butane hydrogenolysis, dehydrogenation and isomerization, *Appl. Catal. A Gen.* 183 (1999) 253–263, [https://doi.org/10.1016/S0926-860X\(99\)00053-8](https://doi.org/10.1016/S0926-860X(99)00053-8).
- [142] H. He, H.X. Dai, K.Y. Ngan, C.T. Au, Molybdenum nitride for the direct decomposition of NO, *Catal. Lett.* 71 (2001) 147–153, <https://doi.org/10.1023/A:1009067507802>.
- [143] M. Nagae, T. Yoshio, Y. Takemoto, J. Takada, Microstructure of a molybdenum nitride layer formed by nitriding molybdenum metal, *J. Am. Ceram. Soc.* 84 (2001) 1175–1177, <https://doi.org/10.1111/j.1151-2916.2001.tb00810.x>.
- [144] F. Lv, H. Ma, L. Shen, Y. Jiang, T. Sun, J. Ma, X. Geng, A. Kiran, N. Zhu, Wearable helical molybdenum nitride supercapacitors for self-powered healthcare smart sensors, *ACS Appl. Mater. Interfaces* 13 (25) (2021) 29780–29787, <https://doi.org/10.1021/acsmi.1c05247>.
- [145] R. Kumar, T. Bhuvana, A. Sharma, Ammonolysis synthesis of nickel molybdenum nitride nanostructures for high-performance asymmetric supercapacitors, *New J. Chem.* 44 (2020) 14067–14074, <https://doi.org/10.1039/d0nj01693d>.
- [146] E. Bertold-Schweickert, M. Mali, J. Roos, D. Brinkmann, *Phys. Rev. B* 30 (1984) 2891.
- [147] D.H. Gregory, Lithium nitrides as sustainable energy materials, *Chem. Rec.* 8 (2008) 229–239, <https://doi.org/10.1002/tcr.20151>.
- [148] K. Chen, R. Pathak, A. Gurung, E.A. Adhamash, B. Bahrami, Q. He, H. Qiao, A.L. Smirnova, J.J. Wu, Q. Qiao, Y. Zhou, Flower-shaped lithium nitride as a protective layer via facile plasma activation for stable lithium metal anodes, *Energy Storage Mater.* 18 (2019) 389–396, <https://doi.org/10.1016/j.ensm.2019.02.006>.
- [149] M.H. Ryou, Y.M. Lee, Y. Lee, M. Winter, P. Bieker, Mechanical surface modification of lithium metal: towards improved Li metal anode performance by directed Li plating, *Adv. Funct. Mater.* 25 (2015) 834–841, <https://doi.org/10.1002/adfm.201402953>.
- [150] W. Sachsz, R. Juza, Über mischkristalle der zusammensetzung (Li, Co)<sub>3</sub>N, (Li, Ni)<sub>3</sub>N und (Li, Cu)<sub>3</sub>N, *Z. Anorg. Allg. Chem.* 259 (1949) 278–290.
- [151] M. Nishijima, T. Kagohashi, Y. Takeda, M. Imanishi, O. Yamamoto, Electrochemical studies of a new anode material, Li<sub>3</sub>-xMxN (M=Co, ni, Cu), *J. Power Sources* 68 (1997) 510–514, [https://doi.org/10.1016/S0378-7753\(96\)02557-8](https://doi.org/10.1016/S0378-7753(96)02557-8).
- [152] N. Tapia-Ruiz, A.G. Gordon, C.M. Jewell, H.K. Edwards, C.W. Dunnill, J.M. Blackman, C.P. Snape, P.D. Brown, I. MacLaren, M. Baldoni, E. Besley, J.J. Titman, D.H. Gregory, Low dimensional nanostructures of fast ion conducting lithium nitride, *Nat. Commun.* 11 (2020) 1–8, <https://doi.org/10.1038/s41467020-17951-6>.
- [153] K. Xie, J. Yang, Q. Zhang, H. Guo, S. Hu, Z. Zeng, X. Fang, Q. Xu, J. Huang, W. Qi, Burning the mixture of graphene and lithium nitride for high-performance supercapacitor electrodes, *Mater. Lett.* 195 (2017) 201–204, <https://doi.org/10.1016/j.matlet.2017.02.129>.
- [154] C. Liu, T. Li, H. Zhang, Z. Song, C. Qu, G. Hou, H. Zhang, C. Ni, X. Li, DMF stabilized Li<sub>3</sub>N slurry for manufacturing self-prelithiatable lithium-ion capacitors, *Sci. Bull.* 65 (2020) 434–442, <https://doi.org/10.1016/j.scib.2019.11.014>.
- [155] J.H. Jeong, Y.H. Kim, K.C. Roh, K.B. Kim, Effect of thermally decomposable spacers on graphene microsphere structure and restacking of graphene sheets during electrode fabrication, *Carbon* 150 (2019) 128–135, <https://doi.org/10.1016/j.carbon.2019.05.014>.
- [156] S. Saha, M. Jana, P. Samanta, N.C. Murmu, N.H. Kim, T. Kuila, J.H. Lee, Investigation of band structure and electrochemical properties of h-BN/rGO composites for asymmetric supercapacitor applications, *Mater. Chem. Phys.* 190 (2017) 153–165, <https://doi.org/10.1016/j.matchemphys.2017.01.025>.
- [157] S. Saha, S. Chhetri, P. Khanra, P. Samanta, H. Koo, N.C. Murmu, T. Kuila, In-situ hydrothermal synthesis of MnO<sub>2</sub>/NiO@Ni hetero structure electrode for hydrogen evolution reaction and high energy asymmetric supercapacitor applications, *J. Energy Storage* 6 (2016) 22–31, <https://doi.org/10.1016/j.est.2016.02.007>.
- [158] R. Kumar, K. Gopalakrishnan, I. Ahmad, C.N.R. Rao, BN-graphene composites generated by covalent cross-linking with organic linkers, *Adv. Funct. Mater.* 25 (2015) 5910–5917, <https://doi.org/10.1002/adfm.201502166>.
- [159] W. Zhang, Functional graphene film macroscopic assemblies for flexible supercapacitor application, *J. Phys. Conf. Ser.* 1168 (2019), <https://doi.org/10.1088/1742-6596/1168/2/022071>.
- [160] C.K. Maity, S. Sahoo, K. Verma, A.K. Behera, G.C. Nayak, Facile functionalization of boron nitride (BN) for the development of high-performance asymmetric supercapacitors, *New J. Chem.* 44 (2020) 8106–8119, <https://doi.org/10.1039/c9nj06284j>.
- [161] S. Saha, M. Jana, P. Khanra, P. Samanta, H. Koo, N.C. Murmu, T. Kuila, Band gap engineering of boron nitride by graphene and its application as positive electrode material in asymmetric supercapacitor device, *ACS Appl. Mater. Interfaces* 7 (2015) 14211–14222, <https://doi.org/10.1021/acsmi.5b03562>.
- [162] B. Xu, F. Wu, R. Chen, G. Cao, S. Chen, Z. Zhou, Y. Yang, Highly mesoporous and high surface area carbon: a high capacitance electrode material for EDLCs with various electrolytes, *Electrochem. Commun.* 10 (2008) 795–797, <https://doi.org/10.1016/j.elecom.2008.02.033>.
- [163] B. Xu, F. Wu, R. Chen, G. Cao, S. Chen, Y. Yang, Mesoporous activated carbon fiber as electrode material for high-performance electrochemical double layer capacitors with ionic liquid electrolyte, *J. Power Sources* 195 (2010) 2118–2124, <https://doi.org/10.1016/j.jpowsour.2009.09.077>.
- [164] H.Q. Li, R.L. Liu, D.Y. Zhao, Y.Y. Xia, Electrochemical properties of an ordered mesoporous carbon prepared by direct tri-constituent co-assembly, *Carbon* 45 (2007) 2628–2635, <https://doi.org/10.1016/j.carbon.2007.08.005>.
- [165] A.B. Fuenes, G. Lota, T.A. Centeno, E. Frackowiak, Templated mesoporous carbons for supercapacitor application, *Electrochim. Acta* 50 (2005) 2799–2805, <https://doi.org/10.1016/j.electacta.2004.11.027>.
- [166] K. Xia, Q. Gao, J. Jiang, J. Hu, Hierarchical porous carbons with controlled micropores and mesopores for supercapacitor electrode materials, *Carbon* 46 (2008) 1718–1726, <https://doi.org/10.1016/j.carbon.2008.07.018>.
- [167] D.W. Wang, F. Li, M. Liu, G.Q. Lu, H.M. Cheng, 3D aperiodic hierarchical porous graphitic carbon material for high-rate electrochemical capacitive energy storage, *Angew. Chem. Int. Ed.* 47 (2008) 373–376, <https://doi.org/10.1002/anie.200702721>.
- [168] A. Mishra, A. Mehta, S. Basu, N.P. Shetti, K.R. Reddy, T.M. Aminabhavi, Graphitic carbon nitride (g-C<sub>3</sub>N<sub>4</sub>)-based metal-free photocatalysts for water splitting: a review, *Carbon* N. Y. 149 (2019) 693–721, <https://doi.org/10.1016/j.carbon.2019.04.104>.

- [169] A. Akhundi, A. Habibi-Yangjeh, Graphitic carbon nitride nanosheets decorated with CuCr2O4 nanoparticles: novel photocatalysts with high performances in visible light degradation of water pollutants, *J. Colloid Interface Sci.* 504 (2017) 697–710, <https://doi.org/10.1016/j.jcis.2017.06.025>.
- [170] A. Alaghmandfard, K. Ghandi, A comprehensive review of graphitic carbon nitride (g-C3N4)-Metal oxide-based nanocomposites: potential for photocatalysis and sensing, *Nanomaterials*. 12 (2022), <https://doi.org/10.3390/nano12020294>.
- [171] W.J. Ong, 2D/2D graphitic carbon nitride (g-C3N4) heterojunction nanocomposites for photocatalysis: why does face-to-face interface matter? *Front. Mater.* 4 (2017) 1–10, <https://doi.org/10.3389/fmats.2017.00011>.
- [172] A. Wang, C. Wang, L. Fu, W. Wong-Ng, Y. Lan, Recent advances of graphitic carbon nitride-based structures and applications in catalyst, sensing, imaging, and leds, *Nano-Micro Lett.* 9 (2017) 1–21, <https://doi.org/10.1007/s40820-0170148-2>.
- [173] J. Yang, X. Zhang, C. Xie, J. Long, Y. Wang, L. Wei, X. Yang, Preparation of gC3N4 with high specific surface area and photocatalytic stability, *J. Electron. Mater.* 50 (2021) 1067–1074, <https://doi.org/10.1007/s11664-020-08654-1>.
- [174] G. Dong, Y. Zhang, Q. Pan, J. Qiu, A fantastic graphitic carbon nitride (g-C3N4) material: electronic structure, photocatalytic and photoelectronic properties, *J. Photochem. Photobiol. C Photochem. Rev.* 20 (2014) 33–50, <https://doi.org/10.1016/j.jphotochemrev.2014.04.002>.
- [175] Y. Wu, Y. Wang, M. Li, Progress in photocatalysis of g-C3N4 and its modified compounds, in: *EEES Web Conf*, 233, 2021, pp. 1–6, <https://doi.org/10.1051/e3sconf/202123301114>.
- [176] L. Xu, J. Xia, H. Xu, S. Yin, K. Wang, L. Huang, L. Wang, H. Li, Reactable ionic liquid assisted solvothermal synthesis of graphite-like C3N4 hybridized  $\alpha$ -Fe2O3 hollow microspheres with enhanced supercapacitive performance, *J. Power Sources* 245 (2014) 866–874, <https://doi.org/10.1016/j.jpowsour.2013.07.014>.
- [177] Q. Chen, Y. Zhao, X. Huang, N. Chen, L. Qu, Three-dimensional graphitic carbon nitride functionalized graphene-based high-performance supercapacitors, *J. Mater. Chem. A* 3 (2015) 6761–6766, <https://doi.org/10.1039/c5ta00734h>.
- [178] Y. Luo, Y. Yan, S. Zheng, H. Xue, H. Pang, Graphitic carbon nitride based materials for electrochemical energy storage, *J. Mater. Chem. A* 7 (2019) 901–924, <https://doi.org/10.1039/c8ta08464e>.
- [179] X. Sun, H. Yang, H. Zhu, L. Wang, Z. Fu, Q. Zhang, H. Zhu, Synthesis and enhanced supercapacitor performance of carbon self-doping graphitic carbon nitride/NIS electrode material, *J. Am. Ceram. Soc.* 104 (2021) 1554–1567, <https://doi.org/10.1111/jace.17529>.
- [180] B. Guan, Q.Y. Shan, H. Chen, D. Xue, K. Chen, Y.X. Zhang, Morphology dependent supercapacitance of nanostructured NiCo2O4 on graphitic carbon nitride, *Electrochim. Acta* 200 (2016) 239–246, <https://doi.org/10.1016/j.electacta.2016.03.175>.
- [181] Q.Y. Shan, X.L. Guo, F. Dong, Y.X. Zhang, Single atom (K/Na) doped graphitic carbon Nitride@MnO2 as an efficient electrode material for supercapacitor, *Mater. Lett.* 202 (2017) 103–106, <https://doi.org/10.1016/j.matlet.2017.05.061>.
- [182] M. Tahir, C. Cao, F.K. Butt, F. Idrees, N. Mahmood, Z. Ali, I. Aslam, M. Tanveer, M. Rizwan, T. Mahmood, Tubular graphitic-C3N4: a prospective material for energy storage and green photocatalysis, *J. Mater. Chem. A* 1 (2013) 13949–13955, <https://doi.org/10.1039/c3ta13291a>.
- [183] R. Gonçalves, T.M. Lima, M.W. Paixão, E.C. Pereira, Pristine carbon nitride as active material for high-performance metal-free supercapacitors: simple, easy and cheap, *RSC Adv.* 8 (2018) 35327–35336, <https://doi.org/10.1039/c8ra06656f>.
- [184] Q. Li, Y. Chen, J. Zhang, W. Tian, L. Wang, Z. Ren, X. Ren, X. Li, B. Gao, X. Peng, P.K. Chu, K. Huo, Spatially confined synthesis of vanadium nitride nanodots intercalated carbon nanosheets with ultrahigh volumetric capacitance and long life for flexible supercapacitors, *Nano Energy* 51 (2018) 128–136, <https://doi.org/10.1016/j.nanoen.2018.06.053>.